The Thesis Committee for Ross Michael Rechen
Certifies that this is the approved version of the following thesis:

Development of a Meso-scale Liquid-Fueled Burner for Electricity Generation Through the Use of Thermoelectric Modules

APPROVED BY
SUPERVISING COMMITTEE:

Supervisor:

Matthew Hall

Ronald Matthews

Development of a Meso-scale Liquid-Fueled Burner for Electricity Generation Through the Use of Thermoelectric Modules

by

Ross Michael Rechen, B.S

Thesis

Presented to the Faculty of the Graduate School of

The University of Texas at Austin

in Partial Fulfillment

of the Requirements

for the Degree of

Master of Science in Engineering

The University of Texas at Austin

May 2011

Dedication

To my parents for always encouraging me in whatever I choose to pursue, to my sister Lindsay who can make me laugh and insult me at the same time, to Ashley for her care and support, and finally to my late grandfather Marvin who first exposed me to engineering in his garage many years ago.

Acknowledgements

I would like to thank Dr. Hall for advising and guiding me throughout this endeavor. I would also like to thank Marlow Industries for providing support to carry out this research. In particular, I thank Joshua Moczygemba and Jim Bierschenk at Marlow for providing ample feedback and direction.

May 6, 2011

Abstract

Development of a Meso-scale Liquid-Fueled Burner for Electricity Generation Through the Use of Thermoelectric Modules

Ross Michael Rechen, M.S.E.

The University of Texas at Austin, 2011

Supervisor: Matthew Hall

The goal of this research was to design, build and test a small burner and heat exchanger system that could be used as a source of heat for thermoelectric modules (TEMs) for the purpose of generating portable electric power for soldiers in the field. The project was conducted as a subcontract to Marlow Industries Inc. which was under contract from the U.S. Army. The scale of the burner thermal output was to be in the approximate range of 2 kW of heat production and it was to be able to operate on a liquid fuel, specifically JP8. The first burner investigated was a custom burner designed and built at UT. It was tested with various fuel and air delivery systems. Different methods to start it, with the goal of developing an electrical starting system, were also investigated. It was capable of operating at outputs over 1 kW, but was difficult to start reliably and fuel vaporization characteristics were sensitive to operating conditions. Two

commercial burners were also studied, each with somewhat different designs. One of those burners, manufactured by MSR, was chosen to be further tested in conjunction with a heat exchanger and thermoelectric modules. The performance of the thermoelectric modules used in this study was determined to be very dependent on an attached resistive load, with a peak power output occurring at approximately 3 ohms. Power output was also determined to increase linearly with increasing temperature difference between the hot and cold sides of the module. Power output followed similar trends as open circuit voltage. The temperatures of the heat exchanger across its width were very uniform, but the accuracy in centering the heat exchanger over the burner could significantly affect temperatures. The time to reach steady state temperatures was relatively insensitive to the length of the heat exchanger. The presence of attached thermoelectric modules reduced the temperature of the heat exchangers and exhaust gas slightly. Reducing the heat exchanger length resulted in higher metal temperatures. Without cooling the cold side of the thermoelectric modules, performance increased while the system was heating up, but then dropped after reaching a peak. Cold side cooling improved thermoelectric performance by increasing its temperature difference. Active cooling with a blower and heat sink provided even better performance than passive cooling using just a heat sink at the expense of a larger parasitic load. The TEMs on the 5 inch long heat exchanger could generate 6.32 W with passive cooling, but active cooling would produce no net power. The 11 inch long heat exchanger could generate 12.8 W with passive cooling, and 16 W net could be generated with active cooling. A heat exchanger efficiency calculation showed that the 16, 11 and 5 inch long heat exchangers were about 94.4%, 93.4%, and 90.7% efficient respectively. This efficiency was defined as the ratio of the heat transferred to the heat exchanger to the heat released in the flame.

Table of Contents

List of Tables

List of Figures

Chapter 1: Introduction

This thesis presents a study concerning the development of a system for thermoelectric electricity generation from a liquid-fueled combustor system. In particular, a system consisting of a meso-scale burner fueled by kerosene, a heat exchanger, and a series of thermoelectric modules was investigated. This chapter explains the motivation behind the present research and provides some background information. In addition, this chapter provides some explanation as to why certain design decisions were made in the development of this burner system.

1.1 MOTIVATION

Most new technologies start their lives unoptimized, for example, being extremely large and heavy. As the technology matures, it inevitably becomes smaller and more portable. This can be seen in everything from computers to cell phones. The physicist, Richard P. Feynman, spoke to the American Physical Society over 50 years ago on this subject [1]. He describes the future miniaturization of many devices and processes. Interestingly, he does not cover the miniaturization of the power sources for these new technologies. It is often the power source that determines the size and weight of portable consumer devices. Today, that power source is inevitably a battery.

Liquid hydrocarbon fuels offer a much higher energy density than even the most advanced batteries. A comparison between the specific energy of two hydrocarbon fuels and various battery technologies is shown in Figure 1.1.

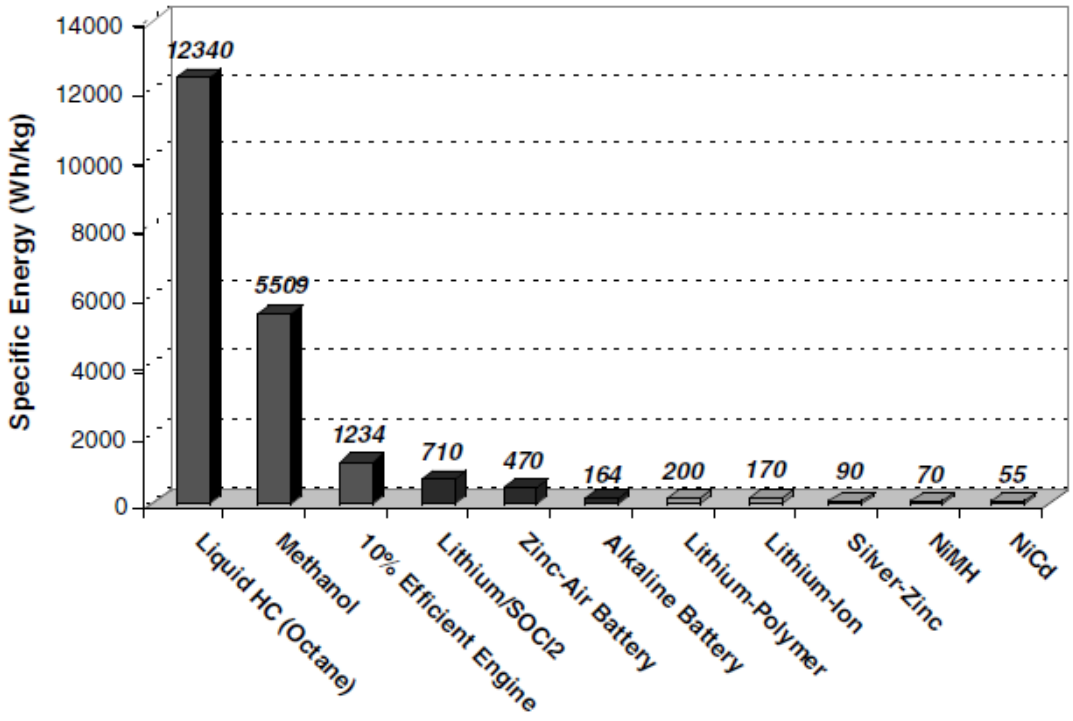

Figure 1.1: Specific energy for octane, methanol, and various battery technologies [2].

Liquid hydrocarbons tend to have a very high specific energy, on the order of 45 MJ/kg [3]. Lithium batteries, which are the best performing batteries currently available, have an energy density of only on the order of 1 MJ/kg. Thus, a system that can convert the chemical energy of a liquid hydrocarbon fuel to electricity with even just 5% efficiency will still be able to outperform the top battery technologies. This is the basis of recent interest in developing a power generation system utilizing a liquid-fueled burner.

One application of such a system would be to provide power to military personnel in the field. A modern soldier carries many electronic devices into the field which inevitably need recharging. This is currently accomplished through the use of batteries. These batteries can be heavy and therefore taxing to move between locations. As previously stated, batteries also have a fraction of the energy density compared to liquid

hydrocarbon fuels. The present study was commissioned to investigate if a generator system containing a liquid-fueled combustor was both a feasible and practical replacement to battery charging.

1.2 MESO-SCALE BURNERS

Meso-scale combustion generally refers to devices having length scales from approximately 1 mm to 10 cm and power generation capabilities on the order of 10 W to 1 kW [4]. The system analyzed in the present study falls within these limits, and therefore can be considered in the meso-scale.

There are many issues seen in the meso-scale that are not encountered with larger burners. As size decreases, the surface-to-volume ratio increases. This ratio is a rough indicator of the ratio between heat loss and heat release rates. Thus, at a small enough size, the losses become so high that combustion cannot be sustained and extinction occurs. In addition, the short flow residence times inherent with small combustors can inhibit complete combustion [5]. These issues are seen in the present study.

1.3 COMBUSTOR TECHNOLOGIES

1.3.1 Catalytic Combustion

As the name implies, catalytic combustion involves the use of a catalyst to aid in the combustion reaction. While it is possible to design an electricity generating system involving a catalytic combustor [6], the present study does not focus on this technology. The existing designs for catalytic combustors are based on fuel flow rates on the order of 10 g/hr [7]. In Kyritsis et al. [5], specific operational limits on the fuel flow rate are stated for their meso-scale catalytic burner. It is stated that a flow rate below 6 g/hr will not allow the reaction to be sustained. A flow rate over 25 g/hr resulted in only a partially premixed flame due to insufficient fuel residence time. Of course, a larger

burner would result in longer residence times and a higher fuel flow rate limit, but that will limit portability. As the present study's heat release rate goal is on the order of 1 kW, and a fuel flow rate of 25 g/hr equates to a heat release rate of only approximately 300 W, catalytic combustion was not investigated further.

There are some advantages to using a catalytic combustor, assuming the required output falls within its operational limits. It is capable of very high combustion efficiencies nearing 99% as well as achieving complete combustion at short residence times. It is stated that another advantage is that the fuel can burn at a lower temperature than in an open flame combustor at the same equivalence ratio. This could be advantageous if the combustor is used in conjunction with an electricity generator, such as a thermoelectric module, requiring narrow temperature ranges [8]. However, introducing a dilutant downstream from an open flame combustor will have a similar effect. Also, the lower temperatures could limit performance depending on the heat exchanger design.

1.3.2 Open Flame Combustion

Open flame combustion is a much more mature and commonplace technology as compared to catalytic combustion. Open flame combustion has been researched for literally thousands of years and has been constantly improved upon. It can be seen in many aspects of everyday life. Most importantly for this study, the heat output limits tend to be higher for open flame combustion as compared to catalytic combustion for burners of similar size. Since the heat output goal of this study is quite a bit higher than any published meso-scale catalytic combustor data, an open flame combustor was chosen to be studied for this system.

1.4 JP8 Fuel and Using Kerosene as a Substitute

This study was performed under a subcontract to the U.S. Army through Marlow Inc. As such, the focus of this study was uniquely directed in some cases. One aspect was the choice of fuel. JP8 is a kerosene-based fuel used in military jets (USAF, NATO, Japanese Self-Defense Forces), tanks and other fighting vehicles, and portable heaters [9]. Therefore, it would be of interest to the military for a portable generator to be fueled by the readily available JP8. As JP8 is a military fuel, it is difficult for civilians to obtain. Store-bought kerosene was used as a substitute. Table 1.1 shows the property data of both JP8 and kerosene.

Property	**JP8**	**Kerosene**
Density (kg/L, 15°C)	0.755 - 0.840	0.8
Boiling Point (°C)	205 - 300	200 - 260
Freezing Point (°C)	-47	-45.6
Flash Point (°C)	38	38
Heat of Combustion (MJ/kg)	42.8	43.1

Table 1.1: Comparison of JP8 [10] and kerosene [11] properties.

The pertinent properties of JP8 and kerosene are similar to each other. The most important property in this case is the heat of combustion, which is almost identical between the two fuels. Also, both fuels have similar volatility. This can be seen in the similarity of the boiling points, freezing points, and flash points. While this study focuses on a kerosene-fueled system, the results can likely be extended to JP8-fueled systems as well without much issue.

1.5 Goals of the Study

The initial goal of this study was to analyze the characteristics of a meso-scale burner operating on liquid fuels. This was accomplished by developing a custom-built burner through much trial and error. Various configurations were studied to optimize the size, output, and parasitic losses in the burner system. In addition, two commercial burners were examined for additional data.

It was also desired to determine the performance characteristics of a thermoelectric generator module. A test rig was assembled to accurately measure the power output of a module at known hot and cold side temperatures, and known loads.

The final, and perhaps most important goal of this study was to investigate the performance of a system combining a liquid-fueled burner for heat production, a heat exchanger, and thermoelectric modules for electricity production. Such a system was built using a commercial burner, heat exchangers of various lengths, and thermoelectric modules that were arranged in various ways and attached to the heat exchanger. Both temperature and power output data were recorded.

1.6 Organization of the Document

This thesis is divided into five chapters. Chapter 2 describes the equipment used in performing this study, and also contains a brief overview of thermoelectric theory. Chapter 3 describes the procedures used in conducting the experiments of this study. Chapter 4 presents the results of this study both qualitatively and quantitatively. Photographs, data plots, and tables are all presented for ease of understanding. Finally, Chapter 5 summarizes the conclusions collected from this study and provides suggestions for future work.

Chapter 2: Experimental Apparatus

This chapter describes the materials used in conducting the present study. It outlines the various burner designs that were considered while conducting this study, as well as the associated devices that are part of the overall burner system. These associated devices include the means for fuel delivery and air delivery. In addition, this chapter describes the heat exchanger used to capture the thermal energy released from the combustion of fuel in the burner, and an oxygen sensor used to determine the equivalence ratio during combustion. Finally, this chapter describes the characteristics of the thermoelectric modules used to convert thermal energy to electrical energy, and touches upon the theory behind them.

2.1 BURNER DEVELOPMENT

2.1.1 Custom Burner

2.1.1.1 Design

A custom burner was designed and built for this study. It initially consisted of a store-bought Soto OD-1R burner designed to be used as a backpacking stove, which was modified by adding a short length of square tube with a closed-off bottom end above the burner, and four sets of small diameter round tube connecting the square tube with the burner. A picture of this design can be seen in Figure 2.1.

Figure 2.1: Photograph of the custom burner.

The square tube with the closed-off bottom was used as a hot impingement plate for the liquid fuel. The combustion air was introduced into the top of the square tube. The idea was that liquid fuel would hit the hot plate and instantly vaporize. That gaseous fuel/air mixture would then be carried by the small round tubes to the burner where it would combust. The impingement plate was kept hot since it was placed right above the burner. The round tubes were brazed into the square tube and press-fitted into the burner to minimize fuel loss.

2.1.1.2 Fuel Delivery

The first method investigated to deliver fuel to the burner was using an automotive fuel injector. The injector can be seen in Figure 2.2.

Figure 2.2: Photograph of the automotive fuel injector.

The injector was placed in the top of the square tube to deliver the atomized fuel to the hot impingement plate where it would then vaporize. However, it was discovered that the initial placement of the injector was too far into the square tube which caused it to get too hot; as a result the fuel partially vaporized before it left the injector. This caused vapor lock to occur, preventing sufficient fuel to be provided to the burner. The solution was to simply raise the injector away from the burner heat source.

The injector requires pressurization of the fuel for proper operation, so a pressurized fuel bottle was used. The bottle was pressurized to approximately 15 psi using a laboratory air supply and regulator. The injector was operated using a function

generator that triggered a periodic pulse of fuel of set duration and interval. This allowed a high degree of fuel flow rate control. A calibration plot for the fuel injector is shown in Figure A.1. Through use of an oscilloscope connected to a current-to-voltage transducer, it was also determined that the injector required a very small amount of power to operate, less than 1 W. The transducer converted the current actually being used by the injector to a voltage that could read by the oscilloscope and then observed. Since the injector was provided with a steady 12 V power supply, multiplying that voltage with the current measured by the oscilloscope yielded a power usage. The area under the two peaks on the oscilloscope display associated with opening and closing the injector were added up to calculate the total energy required to operate the injector. Multiplying that energy with the number of pulses occurring per second yielded the injector power usage. Low parasitic losses are critical for this system. The injector had a maximum flow rate of roughly 5.5 mL/min, which was much higher than needed.

In addition to the fuel injector, a very small fuel pump was investigated for fuel delivery. The injector worked well but requires pressurized fuel and may be subject to coking and clogging. The fuel pump did not have these possible issues. It was discovered that fine atomization of the fuel was not necessary for this burner setup, thus the use of the micropump. This micropump was purchased from Bartels Mikrotechnik and can be seen in Figure 2.3.

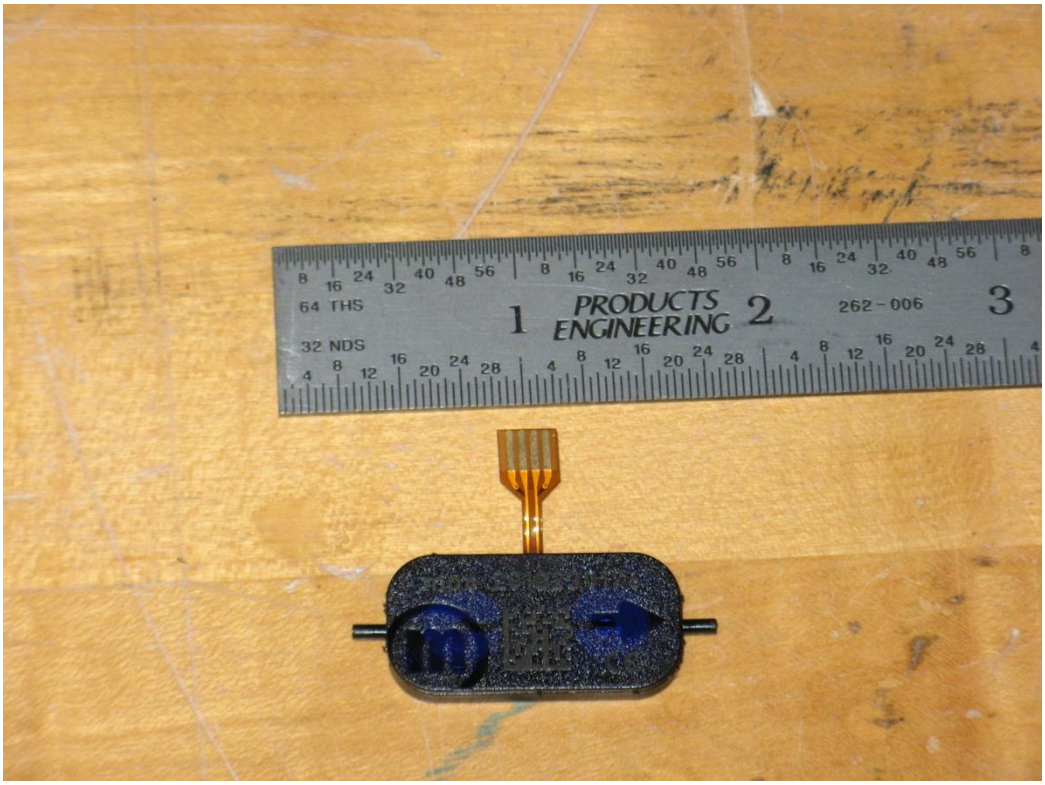

Figure 2.3: Photograph of the small fuel pump with imperial ruler for scale.

It is extremely small at only a bit over one inch in length. It is capable of pumping approximately 6 mL/min of fuel. This fuel flow rate translates to an ideal heat release rate of a bit less than 4 kW, which is on the high end of the goal for this study. The pump literature states that it uses less than 200 mW of electric power [12]. A small diameter plastic tube carried the fuel from its reservoir to the pump, and a second length of the same plastic tube attached to a small diameter metal tube carried the fuel from the pump into the burner through the top of the square tube. The small diameter metal tube was used since the plastic tube would have melted if placed close to the burner heat. Rather than atomizing the fuel as with the injector, the fuel pump simply dripped liquid fuel onto the hot impingement plate where it would quickly vaporize. There was no atomization of

the fuel before it hit a hot surface. From there, the gaseous fuel would be carried to the burner where it would combust.

The controller for the micropump allowed for a great degree of flow rate control. Both the frequency of the pump and its input voltage can be easily varied. Flow rate increases approximately linearly with increasing voltage. However, the frequency at which the maximum flow rate occurs depends on the viscosity of the fluid being pumped. The flow rate increases with increasing frequency until the resonance frequency of the combination of the fluid being pumped and the pump itself is reached. Following that, flow rate decreases with increasing frequency. Calibration curves for this micropump and controller can be seen in Figures A.2 and A.3. The pump controller was relatively large at approximately 7.5 x 16 x 20 cm and thus it would be infeasible to integrate such a sizable controller into a final burner system. A final system would be able to use an available microchip controller supplied by the pump manufacturer integrated into a circuit board.

2.1.1.3 Air Delivery

Regardless of the operating conditions and fuel delivery system used, natural convection alone was not able to provide enough air through the square cross-section tube and the four feeder tubes for a sustainable premixed flame. Thus, several forced air delivery systems were investigated.

Initially, air was provided to the burner system by a compressed air line. The airline was simply inserted into the square tube at the top of the system. The air entrained the vaporized fuel and carried the mixture through the four round tube sections to the base of the burner. The square tube acted as a regenerator to preheat the air prior to mixing with the fuel and entering the burner head. This system was able to provide a

stable premixed flame, but it would not be practical in a final system. Since a goal is for this system to be portable, a compressed air supply is not feasible.

The compressed air source was next replaced by a small electric fan installed above the entrance to the square tube in the burner system. This type of fan is commonly used to cool computer CPUs. It was determined that the fan used only about 1-2 Watts of electric power. The burner system was successfully tested at heat release rates of approximately 500 W. This is towards the lower end of the desired output for this system. While the fan performed about as well as the compressed air supply, it limited the output of the system. The electric fan was not able to provide sufficient air to the burner to ensure a fully premixed flame.

It was calculated that for a fuel flow rate of 5 mL/min, which translates to a heat release rate of approximately 3 kW, about 49 L/min or 1.7 CFM of air is required for stoichiometric combustion. Most CPU-type fans are capable of this flow rate assuming it doesn't have to fight against significant pressure drop. This was not the case for this burner system, however. There was a small but significant pressure drop for air flow passing through the system, particularly the four small tubes leading from the square tube section to the burner body. This type of fan is not capable of providing a large pressure head. A typical value for these devices is 1 inch of water or 249 Pa. An air supply system capable of a larger pressure head was required.

A small blower, which is also known as a centrifugal fan or a squirrel-cage fan was then adopted as a replacement for the electric fan. The blower is shown in Figure 2.4.

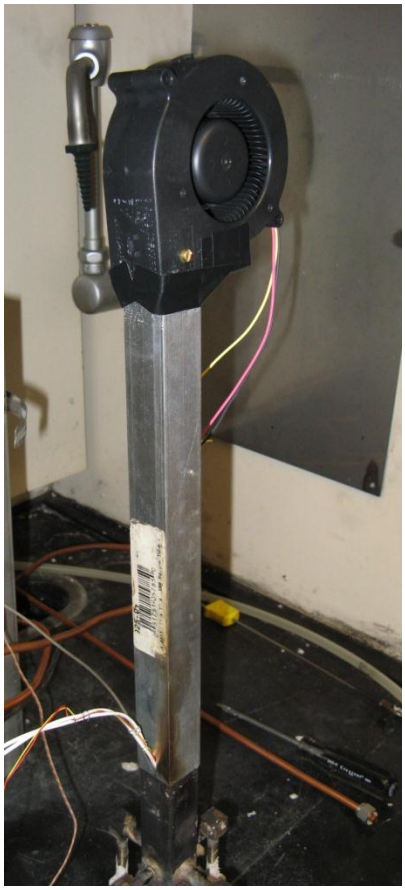

Figure 2.4: Photograph of the duct and blower used for air delivery system.

It was capable of a providing a higher flow rate of air to the burner than the electric fan. It was also capable of providing the air under a bit more pressure to overcome the pressure drop through the burner system. Product literature stated that this blower was capable of an air flow rate of 23 CFM at ambient conditions under no pressure drop while using only about 8 W of electricity. The overall size and weight of the blower were similar to that electric fan.

The blower was successfully tested in the burner system at fuel flow rates up to 6 mL/min, which translates to a thermal power output of about 3.5 kW. Even at this relatively high output, the blower was able to provide enough air to get a stable blue

premixed flame from the burner. This compares favorably to the electric fan that was able to sustain a premixed flame only at heat release rates below approximately 1 kW. The blower speed was controllable by varying the applied voltage from its DC power supply.

2.1.1.4 Start-Up Heat Source

A challenge in developing this burner system was engineering a way to start the system. The closed-off bottom of the square tube, or impingement plate, needed to get hot before liquid fuel could be vaporized by hitting its surface. Initially, the burner system was started by first using a gaseous fuel to pre-heat the system or with a propane torch. It was not desirable to require two different fuels for operation of this system, as would be the case if a gaseous fuel was required for start-up. So, an electrical start system was developed.

A very small square ceramic heater was purchased from Watlow Electric Manufacturing Company for this purpose. It was 0.75 inches square and 0.1 inches thick. It ran on 120 VAC electricity and had a peak power output of 200 W. It was able to reach temperatures of 400°C [13], which is in excess of the final boiling point of kerosene [11]. This heater can be seen in Figure 2.5.

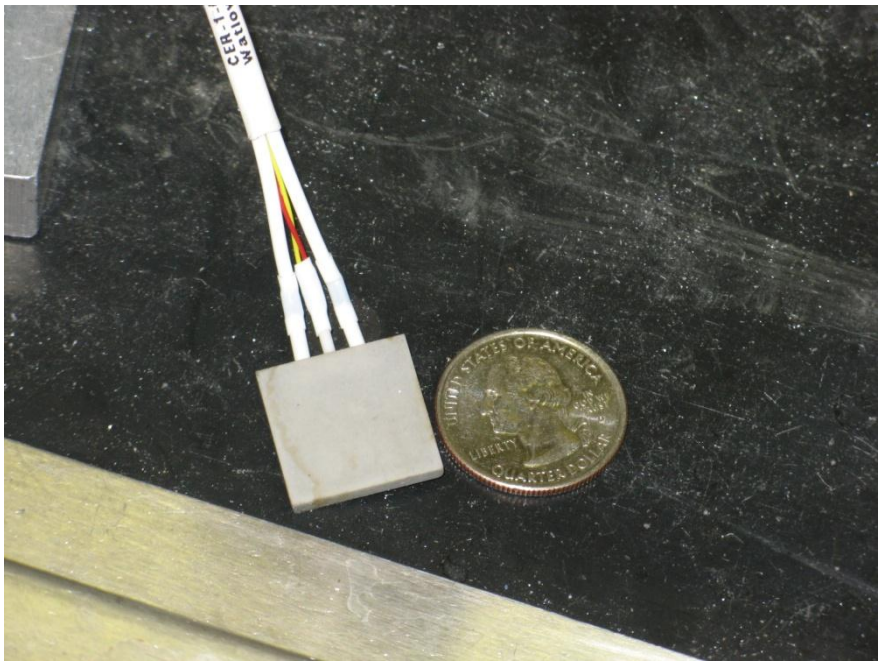

Figure 2.5: Photograph of the small ceramic heater with US Quarter as scale reference.

The ceramic heater was placed inside the square tube of the burner system, where it rested on the impingement plate at an angle. During start-up, fuel would hit the hot heater and vaporize. The gaseous fuel then was carried to the combustion chamber of the burner and ignited. After the system ignited, power to the heater was stopped. From then on, fuel would first hit the inclined heater and then run down to the hot impingement plate below it to vaporize in steady-state operation. The heater contains a K-type thermocouple to monitor its temperature.

2.1.2 Brunton Burner

In addition to the custom burner system designed and built for this study, two commercial burners were also evaluated. One of these was the Brunton Vapor AF All Fuel Expedition Stove [14]. This burner can be seen in Figure 2.6.

Figure 2.6: Photograph of the Brunton commercial burner.

The unique feature on this particular burner is the impingement plate hanging above the burner cup seen in the above figure. After a warm-up period where liquid fuel is burned within the combustion cup at the base of the burner in a non-premixed fashion, fuel jets upward from a small nozzle and hits the now-hot impingement plate. There, is it instantly vaporized and burned. The fuel is delivered to the burner by way of pressurization of the fuel bottle. Air was supplied by entrainment through holes in the body of the burner. It was able to produce a steady blue premixed flame for an extended period of time while running on liquid fuel at a heat release rate of approximately 1.5 kW. This burner was not used in further experimentation.

2.1.3 MSR Burner

2.1.3.1 Design

The other commercial burner used in this study was the MSR Whisperlite Internationale stove [15]. It can be seen in Figure 2.7.

Figure 2.7: Photograph of the MSR commercial burner.

Like the Brunton burner [14], this burner also uses a hot impingement plate to vaporize the liquid fuel. It also delivers fuel to the burner through a pressurized fuel bottle, and air is naturally entrained through holes in the burner. However, it employs an additional unique feature in that it preheats the incoming liquid fuel by passing the fuel line through the open flame. This recuperation method aids in the vaporization of the liquid fuel. Its heat release rate was measured at approximately 2 kW. This burner was used in further testing due to its additional sophistication over the other commercial burner.

2.1.3.2 Electric Start System

Further testing with the MSR burner first required refinement of its start-up characteristics. Like the Brunton burner, a small pool of liquid fuel needed to be burned in a relatively large and sooty diffusion flame to heat up the burner's impingement plate before it could produce a steady blue premixed flame. This was unacceptable in a final system, or even for testing. Thus, an electric start-up system was engineered.

The small square ceramic heater [13] was used as one part of the system. A small cartridge heater was used as the other part. The ceramic heater was placed underneath and in contact with the burner body. This was to heat the body of the burner, and particularly the fuel nozzle. The cartridge heater was strapped to the fuel line as close as possible to the fuel nozzle to heat the incoming fuel. This simulated the effect of having the fuel line pass through the burner flame during normal operation. These two electric heaters used in conjunction were able to start up the MSR burner without the need for non-premixed burning of liquid fuel.

2.2 HEAT EXCHANGER

In order to capture as much thermal energy as possible from the combustion of the liquid fuel in the burner, a heat exchanger was developed. The heat exchanger also provided a surface to attach thermoelectric modules and convert some of the thermal energy to electrical energy.

2.2.1 Design

The heat exchanger was constructed from four extruded aluminum heat sinks with a cross-section 4.23 inches wide and 1.05 inches tall. This cross-section can be seen in Figure 2.8.

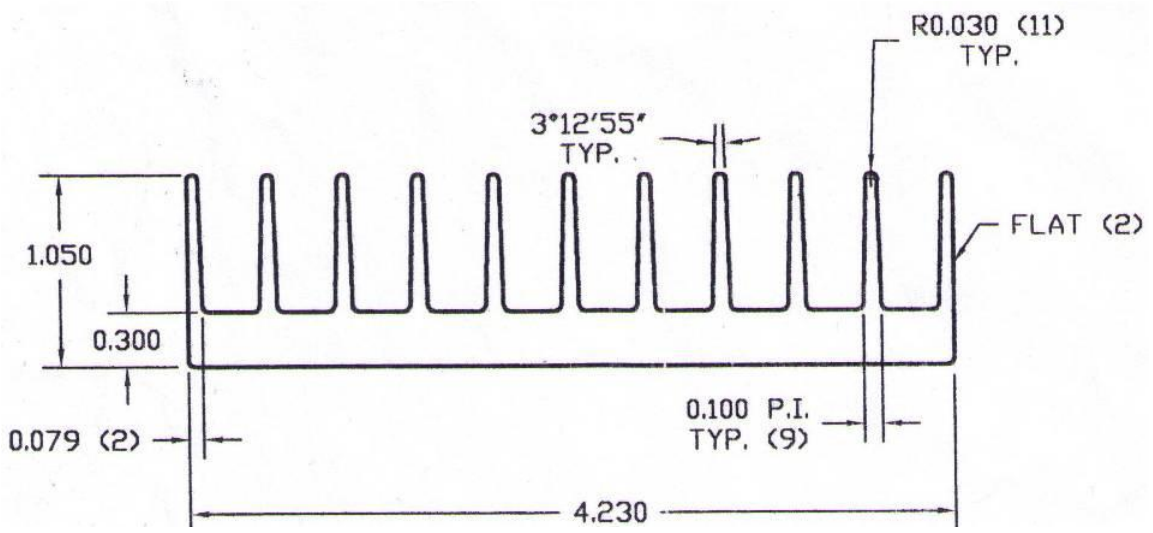

Figure 2.8: Technical drawing of the cross-section of the heat sink used to construct the heat exchanger [16].

The heat sinks were purchased at a 16 inch length, to ensure that as much energy as possible was captured. To construct the heat exchanger, 45-degree chamfers were cut into both sides of the cross-section for each of the four heat sinks. When fitted together with hose clamps securing it, the four heat sinks formed a square cross-sectioned box with an open top and bottom. The idea was for the heat exchanger to surround the burner and route as much exhaust as possible through it without letting in entrained air, which then left out the top to the atmosphere. The fins acted as extended surfaces to enhance the heat transfer to metal, and then to the thermoelectric modules. Testing revealed that plugging up the center of the heat exchanger improved performance. The hot gases were forced to flow through the finned area. The center plug was constructed with a core of solid alumina ceramic with alumina silica ceramic fiber packed on top of it. Figure 2.9 shows this plug along with the cross section of the assembled heat exchanger.

Figure 2.9: Photograph of the cross-section of the assembled heat exchanger with ceramic fiber core.

As can be seen in the above figure, the center fins of each heat sink were milled off to a minimal depth. This was to accommodate the four sets of small tubes in the custom burner when the heat exchanger was placed over it for testing. Later on, the heat exchanger was cut into two unequal lengths of approximately 11 inches long and 5 inches long. This was to determine an optimal length to capture a maximum amount of heat while keeping the system as compact as possible. This was also done to determine the correlation between heat exchanger length and maximum temperature since the thermoelectric generators had a maximum temperature limit. These devices are discussed later. The weight of the 16, 11, and 5 inch long heat exchangers were approximately 4.7 kg, 3.3 kg, and 1.5 kg respectively.

2.2.2 Heat Exchanger Temperature Measurement

A series of K-type thermocouples were used to determine the temperature of the heat exchanger in both the axial direction and across its width. Since the heat exchanger was 90-degree rotationally symmetric, measuring the temperatures on only one heat sink was sufficient to characterize the temperatures for the whole heat exchanger. The thermocouples were purchased from Omega Engineering and are of the bolt-on washer type. Small threaded holes were drilled and tapped on one of the four outer sides of the heat exchanger to attach the thermocouples with screws. A Stanford Research Systems 16-channel thermocouple monitor was used to measure the temperatures of the thermocouples. The full length heat exchanger with attached thermocouples is shown in Figure 2.10. Additional thermocouple attachment holes were drilled and tapped after the heat exchanger was cut into two pieces to allow for better resolution of the temperature data.

Figure 2.10: Photograph of the full length heat exchanger with attached thermocouples.

As seen in the above photo, at one point the tapped hole for the top thermocouple was enlarged and re-tapped to allow insertion of the UEGO sensor discussed in the next section. A rubber stopper was used to seal the heat exchanger when the UEGO sensor was not used.

2.3 UEGO SENSOR

A UEGO (Universal Exhaust Gas Oxygen) sensor was used to determine the combustion equivalence ratio of the burners. It was inserted through a tapped hole in the heat exchanger wall so that the sensor was in the exhaust stream of the burner. The output of the sensor was a voltage that was measured by a multimeter. Through the use

of a calibration chart, seen in Figure A.4, this voltage was converted to an equivalence ratio. This allowed the air flow rate through the heat exchanger to be determined from the measured fuel/air equivalence ratio and the known fuel flow rate. The fuel flow rate of the burner was easily determined by measuring the volume flow rate of liquid fuel. Dividing the stoichiometric amount of air required for one mole of fuel with the equivalence ratio yielded the molar amount of air passing through the burner for every mole of fuel burned. This could be easily converted to a mass basis by utilizing the molar masses of the air and fuel. The UEGO sensor is seen in Figure 2.11.

Figure 2.11: Photograph of the UEGO sensor.

2.4 THERMOELECTRIC GENERATOR

A goal of this study was to convert the chemical energy contained in liquid fuels to electrical energy. The way to accomplish this was to use thermoelectric modules. They are capable of directly generating electricity from a temperature difference without

the need for moving parts. That is very desirable for a portable system; there is less chance for a malfunction and less need for preventative maintenance relative to a Stirling engine.

2.4.1 Thermoelectric Theory

A typical thermoelectric device consists of a junction formed from two different semiconductor materials. One of the materials contains negative charge carriers (n-type), and the other contains positive charge carriers (p-type). When a temperature gradient is applied across the junction, electron-hole pairs are created at the hot end and recombine at the cold end. This results in an electrical potential between the hot and cold ends of the thermoelectric device. This effect, known as the Seebeck effect, allows these devices to be used as power generators.

The voltage that is generated by a thermoelectric device when a temperature gradient is applied is given by

$$V = \int_{T_1}^{T_2} [S_A(T) - S_B(T)] dT \tag{2.1}$$

where S_A and S_B are the Seebeck coefficients of the two materials used to form the device, and T is the temperature. T_1 and T_2 are the cold and hot side temperatures of the thermoelectric device.

The efficiency of the thermoelectric device is generally expressed by a term known as the figure of merit (Z), which is defined as

$$Z = \frac{S^2}{\rho k} \tag{2.2}$$

where S is the Seebeck coefficient of the material, ρ is the electrical resistivity of the material, and k is the thermal conductivity of the device. This value can be nondimensionalized by multiplying Z with the average temperature (ZT). A device with

a higher ZT value is more efficient at converting heat to electricity, and most modern commercial devices have a ZT value of no more than 1 [17].

A thermoelectric device should be integrated into a system such that it is exposed to the maximum allowable temperature difference between its two faces. The hot side temperature is generally limited to approximately between 200°C and 300°C. This limit is defined by both the melting and degradation of the materials used in the device or its packaging, and by mitigation of the dopants in the semiconductor components of the device. As such, a device will generate the maximum amount of power if its hot side is uniformly at the maximum allowable temperature and the cold side is uniformly at the lowest practical temperature [18].

2.4.2 Thermoelectric Module Design and Specifications

A series of thermoelectric power generators were provided for use in this study by Marlow Industries (model number TG 12-8-01L). Each module is 1.58 inches wide by 1.76 inches long with a height of 0.143 inches. They are manufactured with Bi_2Te_3 semiconductor material. The manufacturer stated that the maximum allowable temperature for these units is 250°C for short periods of time, and a maximum of 230°C for prolonged use, due to melting of solder joints. This was the target hot side temperature in testing these modules to achieve the maximum possible power generation. It was also stated that the ZT for each of these devices is 0.73, the optimum efficiency is 4.97%, and the optimum power output is 7.95 W [19].

2.4.3 Individual Module Testing Apparatus

A simple apparatus was built to test the performance of individual thermoelectric modules at varying hot and cold side temperatures, and load resistances. This apparatus can be seen in Figure 2.12.

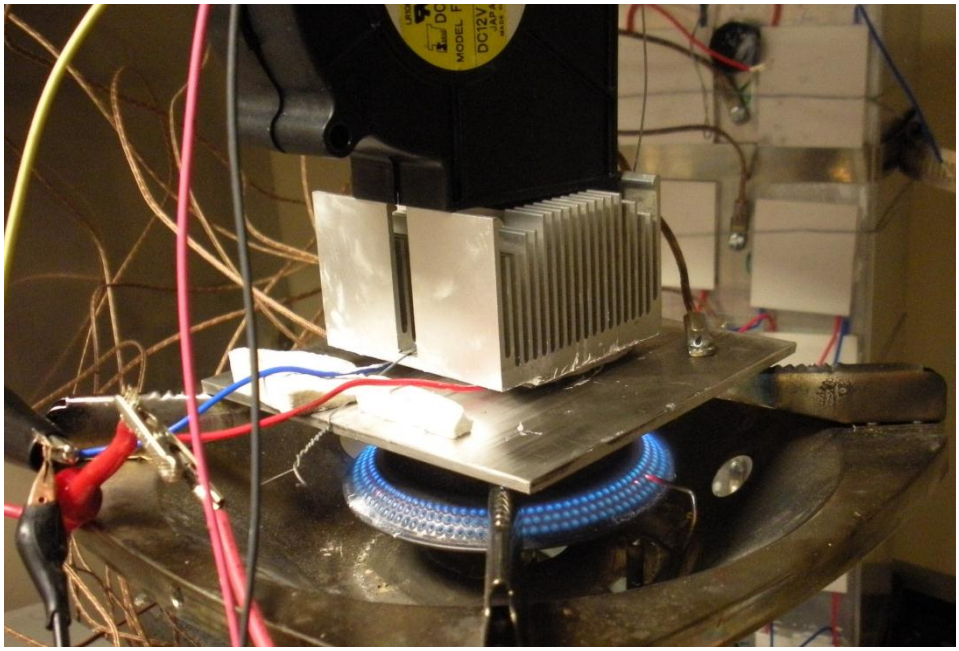

Figure 2.12: Photograph of the apparatus to test individual thermoelectric modules.

A thin aluminum plate was placed over a propane burner to act as the applied heat source to the module. A thermocouple was attached to the plate to monitor its temperature. The thermoelectric module's hot side was adhered to the plate with Chemplex 1381 Heat Sink Compound to improve heat transfer between the plate and module. A CPU-style heat sink was placed on top of the module's cold side and adhered with additional heat sink compound. A blower of the same type used as the custom burner's air delivery system was placed on top of the heat sink to minimize the cold side temperature of the module. The output wires of the module were attached in series to a variable electric resistor to vary the load on it from 1 to 1000 ohms. The output voltage and current of the thermoelectric module was measured by two multimeters. A third multimeter measured the resistance of the variable resistor. This identical setup was used with an electric hot plate in place of the propane burner to test with lower hot side temperatures. The manufacturer does provide some performance data, but it appears to be recorded under

ideal circumstances in a pure nitrogen environment. The manufacturer also only provides data for a select few cold side temperatures and a narrow range of load resistances. It was desired to obtain more "real-world" performance data at a wide range of conditions with this testing.

2.4.4 Thermoelectric Modules Used with the Heat Exchanger

Twelve thermoelectric modules were attached with heat sink compound and steel wire to one outer face of the full length heat exchanger. The previously attached thermocouples were left on. This is shown in Figure 2.13.

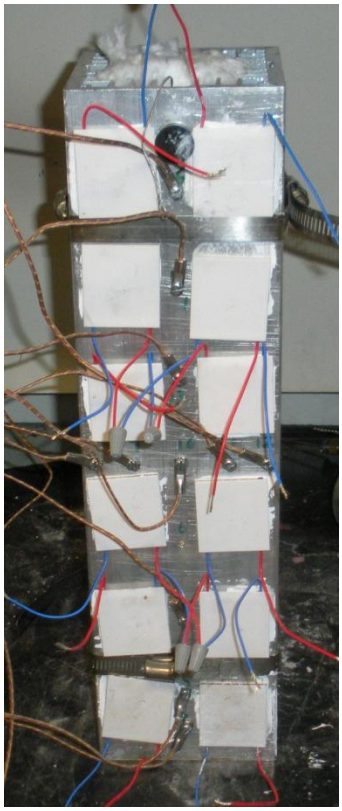

Figure 2.13: Photograph of the full length heat exchanger with attached thermoelectric modules and thermocouples.

The hot side of the modules contacted the heat exchanger. Each row of two modules was connected in series to each other. A CPU-style heat sink was attached to one of the modules. This is not shown in the above figure. This was to determine by how much cold side cooling would improve thermoelectric performance. Heat sink compound was used to attach the thermoelectric modules to the heat exchanger, and to attach the CPU-style heat sink to the module.

For the shorter 5 inch and 11 inch long heat exchangers, additional extruded aluminum heat sinks were purchased to be used for cooling of the cold side of the thermoelectric modules. These additional heat sinks are of the same design as the pieces used to construct the heat exchanger, and a technical drawing of their cross-section can be seen in Figure 2.9. A photograph of this setup for the 5 inch long heat exchanger is shown in Figure 2.14.

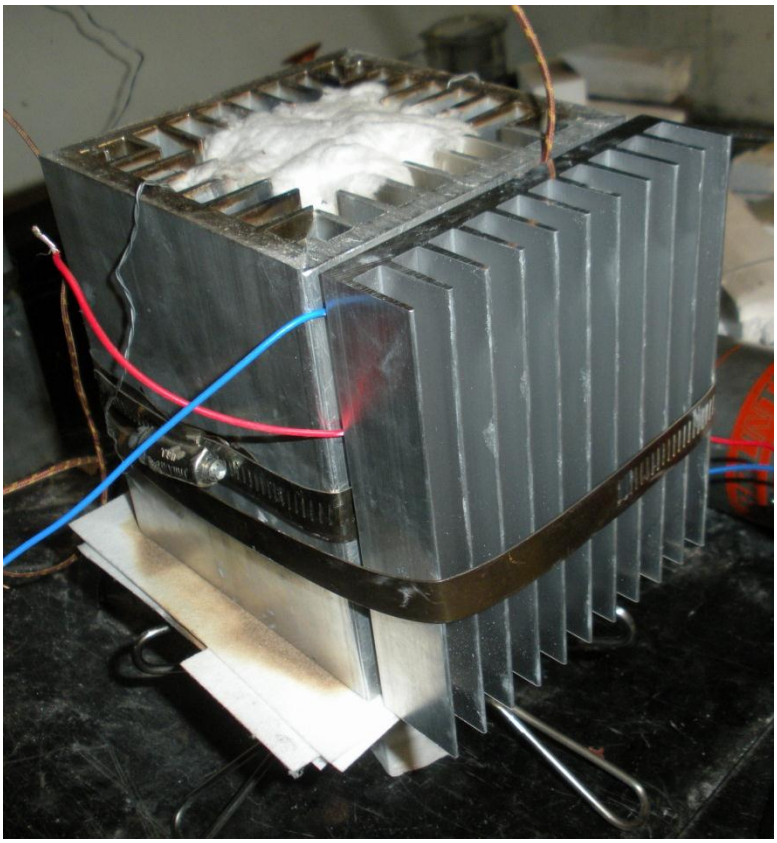

Figure 2.14: Photograph of the 5 inch long heat exchanger with additional extruded aluminum heat sink for cooling the cold side of the thermoelectric modules.

Heat sink compound was applied to both sides of thermoelectric modules, which were then sandwiched between the heat exchanger and the cold side heat sink. An additional hose clamp was used to secure the heat sink to the rest of the heat exchanger. A blower of the same design as seen in Figure 2.4 was used to actively cool the heat sink to see what if any effect that would have. This is shown in Figure 2.15 for the 5 inch long heat exchanger.

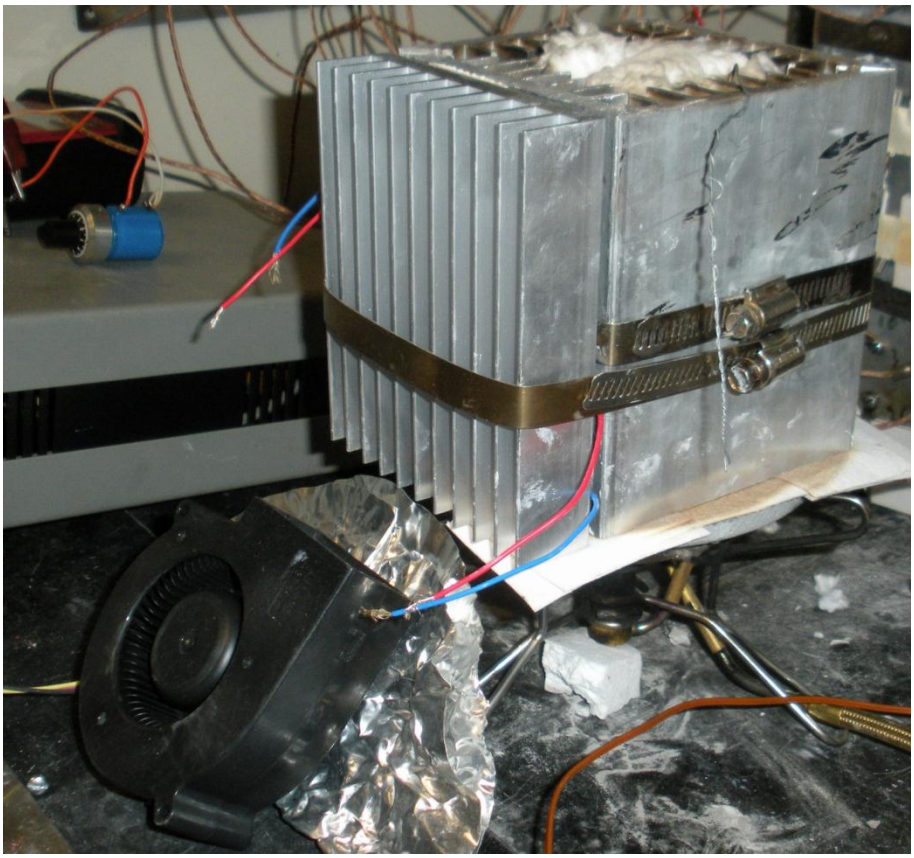

Figure 2.15: Photograph of the 5 inch long heat exchanger with active cooling.

As there was not sufficient room between the heat exchanger and heat sink to attach the bolt-on washer type thermocouples, temperatures were measured using a hand-held thermocouple probe at the top and bottom edges of the heat sink and heat exchanger. A washer type thermocouple was inserted snuggly in the gap containing the thermoelectric modules to provide an average temperature reading between heat exchanger and heat sink so as to indicate when steady-state has been reached.

Chapter 3: Experimental Procedures

This chapter describes the procedures used in this study. It begins with detailing the operation of the custom burner, which includes the various methods to start it up and operating it using various fuel delivery devices. The procedures used to operate the commercial burner under start-up and steady-state conditions are then described. Finally, this chapter informs about the experimental procedures used when running the burner system with the heat exchanger and thermoelectric modules.

3.1 Custom Burner Operation

3.1.1 Start-Up

Starting the custom burner proved to be a challenging aspect of this study. Initially, the custom burner was started using a gaseous fuel canister typically used for camping. The burner was attached to the fuel canister through a standard connector on the bottom of the burner. The burner was first ignited running purely on the gaseous fuel: an isobutane/propane mix. This was to heat the impingement plate that would vaporize the liquid fuel. It was determined that after approximately one minute, the impingement plate was sufficiently hot, so the liquid fuel flow was initiated. The fuel vaporized and was carried to the combustion chamber by the running air supply. The vaporized liquid fuel was ignited by the already present gaseous fuel flame. The flow rate of the liquid fuel was initially very low in order to not cool the impingement plate too greatly. The liquid fuel flow rate was gradually increased while decreasing the gaseous fuel flow rate until the system was operating solely on liquid fuel. This operation required a lot of "feel" and careful observation of the burner flame. Using the gaseous fuel one was able to reliably start the custom burner system, but it was impractical to require two different types of fuels for operation.

Until a way to start the custom burner system without the gaseous fuel was discovered, a propane torch was used. The torch was pointed directly at the bottom of the impingement plate to heat it past the boiling point of the liquid fuel. Once the plate reached a high enough temperature, taking approximately one minute, the liquid fuel flow was turned on at a small flow rate that was gradually increased. The propane torch was also used to ignite the vaporized liquid fuel since there was not already a flame present. This procedure still required the use of two different fuels to operate the burner, which is undesirable. However, the actual procedure was a great deal simpler. It did not require any careful observation or variation of two fuel flow rates; the impingement plate was simply heated above a critical temperature before starting the liquid fuel flow.

An electrical start-up system was greatly preferable to using a secondary fuel, as long as the system was not too large of a parasitic loss. The small square ceramic heater was used for this purpose. The heater was placed at an angle inside the square tube portion of the burner system. It was connected to a variable AC power supply. It was found that powering the ceramic heater for about 1 minute at 35% of the power supply's capacity, translating to 17 W of power and a total of 1020 J of energy, was able to get the heater sufficiently hot for liquid fuel to vaporize on contact. With the air supply operating, it was easy to tell if the heater was hot enough because white fuel vapor would start to flow out of the burner head. In preliminary testing of the ceramic heater it was noticed that if it was too hot a Leidenfrost effect would appear preventing rapid vaporization of the fuel. Care was taken to ensure that the heater was hot enough to vaporize the liquid fuel on contact, but not so hot as to cause the fuel to bead up due to the Leidenfrost effect. This was accomplished through careful monitoring of its temperature through its built-in thermocouple. After the system was ignited, power to the ceramic heater was stopped, and fuel ran down the inclined heater to the now-hot

impingement plate. Ignition of the fuel was accomplished by use of the propane torch only for testing purposes. An electrical sparker or glow-plug would be preferable for use in a final unit. This start-up method proved to be reliable, and didn't require an additional power source since a final unit would contain thermoelectric generators and batteries storing excess generated power to run the ceramic heater.

3.1.2 Steady-State

The difficulty in operating the custom burner was mainly due to the start-up procedures. Once it reached steady-state operation, there wasn't much issue to keeping the burner running. This is at least partially due to the recuperative nature of the burner, in that the heat from the burner heats its impingement plate to vaporize the liquid fuel, which then is carried to the combustion chamber to release more heat.

Regardless of the air supply and fuel supply systems used in operation of the burner, the flow rates of each needed to be carefully monitored in order to achieve a roughly stoichiometric premixed flame. Generally, the fuel flow rate was selected based on the calibration curves for the injector and micropump seen in Appendix A. The air flow was altered until a premixed flame was seen. This was accomplished almost entirely by visual observation. Too little air produced a large yellow diffusion flame and too much air extinguished the flame entirely.

That is not to say that the fuel flow rate wasn't able to be altered during operation of the burner. When using the automotive fuel injector, the flow rate was altered by changing the time between the pulses of the injector on the signal generator. A change was almost immediately seen in the burner flame; decreasing the time between pulses resulted in a larger flame and vice versa. It should be noted that the flame produced by the burner system when using the injector was not fully steady, even though it was at a

steady-state operating condition. Since the injector provided the fuel in a series of pulses, or squirts, the flame appeared to grow and shrink many times a second corresponding to how much time was elapsing between pulses.

Altering the fuel flow rate when using the micropump was more straight-forward. The frequency setting on the pump controller was kept at the pump resonance frequency for kerosene. It was determined to be 150 Hz after recording the flow rate provided by the pump at various frequencies for a constant input voltage and determining its maximum, seen in Figure A.2. The manufacturer states that the frequency of the upstroke and downstroke of the pump affects the fluid flow rate, and the maximum flow rate at a given voltage and for particular fluid occurs at the resonance frequency [20]. The fuel flow rate then was able to be changed by increasing or decreasing the voltage passed to the pump from the controller. Since it was found that the flow rate had a linear dependence on the voltage, this was not an issue. As with the injector, a change in fuel flow rate from the micropump resulted in an almost immediate change in the size of the burner flame. Unlike the injector, the flame was steady due to the constant flow of fuel provided by the pump.

3.2 Commercial Burner Operation

The procedures for operating only the MSR burner [15] and not the Brunton burner [14] are discussed in this section since only the MSR burner was used for further experimentation beyond simply observing its technology. However, procedures for running either commercial burner are rather similar to each other.

3.2.1 Start-Up

The MSR burner package included instructions on how to start-up and run the burner. It stated to open its fuel value for a few seconds, after filling the fuel bottle and

pressurizing it with a built-in air pump, in order to let a bit of liquid fuel run from the burner nozzle to a collecting cup attached to the bottom of the burner. The collected fuel was then ignited by a lighter or torch and left to burn resulting in a large, sooty, and yellow diffusion flame. That diffusion flame heated the burner's fuel line and impingement plate so that the liquid fuel would vaporize after leaving the fuel nozzle. Once the diffusion flame started to die down, the fuel valve was opened fully and soon produced a blue premixed flame. This method of starting the commercial burner was not acceptable.

To develop a more elegant starting system for the MSR burner, experiments were run to determine which parts of the burner were most critical to heat. A propane torch was used as the heat source for this study. The collecting cup was removed prior to these experiments since it was just additional metal that would need to be heated and served no purpose. The torch was focused on one area of the burner for each run before turning on the fuel flow and igniting it. The parameter of interest was how quickly the burner would produce a blue flame. It was determined that the burner would always produce a blue flame after some time if the fuel nozzle was sufficiently hot. However, it was also determined that heating the fuel line in addition to the nozzle allowed the burner to almost instantly produce a blue premixed flame. Heating the top impingement plate of the burner had no discernible effect on how long before a blue flame was observed.

Thus, based on what was learned from testing with the propane torch, and electric start system was developed for the MSR burner. The small square ceramic heater was placed under the burner so that the burner body was resting on it. This was to heat the nozzle of the burner. Good contact between the burner and heater needed to be maintained to achieve adequate heat transfer. This was accomplished by tightly tying the heater to the burner using some small gauge steel wire. The burner's fuel line was heated

by tying a small cartridge heater onto it, again using some steel wire. In addition, the fuel line and cartridge heater were encased by ceramic blocks to limit the amount of heat escaping to the environment.

Before starting the burner, both the ceramic heater and the cartridge heater were turned on to heat the nozzle and fuel line. After approximately two minutes of preheating, the fuel valve was fully opened allowing fuel to flow into the burner. If the fuel line and nozzle were sufficiently hot, white vaporized fuel was released out the top of the burner. This was an easy way to tell if sufficient preheating time elapsed. Upon seeing the vaporized fuel, the burner was ignited by a propane torch. A sparker or some other heat source would have the same result. The burner then quickly produced a blue premixed flame. There were occasionally a few quick flickers of yellow flame right after igniting the fuel, but they disappeared rapidly.

3.2.2 Steady State

As with the custom burner, the main difficulty in operating this commercial burner was in the start-up procedures. Again, this is due to its recuperative design. The burner flame preheated the fuel in the fuel line before reaching the burner, which also had the effect of keeping the nozzle warm. The flame also heated the burner's impingement plate so that the fuel can be vaporized. Once the commercial burner was ignited and a premixed flame was established, the burner was able to consistently produce the same output until the fuel in its fuel bottle was exhausted.

However, unlike the custom burner, there was no way to change the fuel flow rate for this burner. The valve could be opened or closed without much ability to be set in between. After all, this was a burner designed to be easily used by campers for cooking, so a variable flow control added an unnecessary level of complexity. Even so, the output

of the burner fit well within the design goals of this study at approximately 2 kW. The lack of flow rate control did not prove to be an issue.

3.3 Testing the Performance of an Individual Thermoelectric Module

The procedures for testing the performance of a thermoelectric module were similar whether the heat source was a propane burner or an electric hot plate. After the module was adhered to the plate over the heat source with heat sink compound, the cold side heat sink and blower were attached to the module. The module leads were attached to a variable resistor and multimeters measuring the voltage and current of the module, and the resistance of the variable resistor. The heat source and cold side blower were then turned on. The temperature of the plate over the propane burner was measured by an attached thermocouple, and the hot plate temperature was measured by a hand-held thermocouple probe. The cold side temperature was measured by a hand-held probe in both cases. Once the hot side reached a desired temperature, the load on the system was varied from 1 to 1000 ohms by turning the variable resistor. The current and voltage were recorded at each load to obtain power outputs. The hot side and cold side temperatures, and the open circuit voltage were also recorded. After cycling through all loads, the heat source intensity was altered to achieve new hot and cold side temperatures, and the data acquisition procedure was repeated.

3.4 Operating the Burner System with the Heat Exchanger

Other than some proof-of-concept testing, most of the testing involving the heat exchanger used the commercial MSR burner [15]. It was found that this commercial burner allowed for easier operation than the custom burner, and was more reliable. The only downside was that the fuel flow rate was not able to be controlled while using this

commercial burner. However, as was just mentioned, the output of this burner fell within the design goals of this study.

3.4.1 Preparation

Before igniting the burner, a metal flange was tightly fit around its burner head to direct as much heat as possible upward and through the heat exchanger. It also served as a flat surface for the heat exchanger to rest upon.

Several strips of Cotronics Ultra Temp 390 ceramic paper [21] were placed on top of the flange to reduce the amount of heat conducted between the flange and the heat exchanger. The ceramic paper also served to limit the amount of air that was entrained in the burner exhaust stream. A higher amount of entrained air would lower the temperature of the exhaust gas, thereby decreasing the amount of heat transferred to the heat exchanger. The paper served as a gasket between the heat exchanger and flange producing a tighter seal than just metal-on-metal.

3.4.2 Transient Operation

After the burner was ignited and producing a steady-state premixed flame, the heat exchanger was placed on top of the burner centering it over the burner flame. As the heat exchanger heated up, the temperatures of one of its outer surfaces was measured by the attached thermocouples and recorded. Only the temperatures of the thermocouples at the top and bottom of the heat exchanger were monitored. These measurements were taken every minute at first, and later every few minutes, until the temperature reached steady-state and so did not change with time. Steady-state was defined for these measurements as less than one degree Fahrenheit change per minute. Such a definition was necessary to limit the time required to complete these measurements to a reasonable amount. These measurements were taken with the thermoelectric modules attached and

without them attached. They were also taken for all the heat exchangers of varying lengths.

3.4.3 Steady-State Operation

After the heat exchanger reached steady-state, temperature measurements were taken from all of the attached thermocouples to determine the temperature profile of the heat exchanger along its height and width. The exhaust gas temperatures from the burner were also recorded. A long and rigid K-type thermocouple was inserted into the heat exchanger through its top and held by hand. Temperatures were recorded from a thermocouple monitor for various distances from the bottom of the heat exchanger. The bottom of the heat exchanger was located approximately one inch from the burner flame. These measurements were taken for all of the three different length heat exchangers when the thermoelectric modules were not attached, and only for the full length heat exchanger with attached thermoelectrics.

Additional steady-state data were recorded when the thermoelectric devices were attached to the full length heat exchanger. The hot side temperatures of the generators were determined from the thermocouples attached to the heat exchanger, but the cold side temperatures had to be separately measured. A hand-held K-type thermocouple probe was held against the cold side of each generator so that its temperature could be read. There were two modules at each height on one face of the heat exchanger, and the temperature of only one generator at each height along the heat exchanger was measured since the system is symmetric about the vertical. The open circuit voltage of each row of two modules, which were connected in series, was measured with a multimeter. Also, when one of the two thermoelectric modules in a row had a heat sink on its cold side, the voltage and cold side temperatures were measured for each of the two modules.

For the shorter heat exchangers with attached thermoelectric modules, the procedure was altered due to the presence of the additional extruded aluminum heat sink. There was insufficient room to attach the full array of thermocouples to monitor the temperature of the heat exchanger. So, a thermocouple was inserted between the heat exchanger and heat sink to measure the average temperature between the two metal surfaces. This setup was shown in Figure 2.14; the thermocouple wire is sticking out of the top and the thermoelectric leads protrude from the side. This temperature was monitored to indicate when steady-state was reached. Then, the open circuit voltage, and the voltage and current under load were measured with a multimeter for each of the attached thermoelectric modules. The hot side and cold side temperatures were measured with a hand-held temperature probe pushed firmly into the heat exchanger or heat sink. The exhaust gas temperatures were measured as described at the beginning of this section.

Chapter 4: Results and Discussion

This chapter now presents the results of this study. It begins with a qualitative overview of the performance of the various types of burners experimented with for this study. Next, the results of the single thermoelectric module testing that compare power output with resistive load and temperature difference are shown. The thermal and power generation results of the heat exchanger testing follow. Then, balance-of-plant analysis is presented. Finally, the results from the UEGO sensor leading to heat exchanger efficiency calculations and results are offered.

4.1 Qualitative Burner Results

A significant amount of time invested in this study was devoted to developing and optimizing the actual burner in the overall system. The results gathered from this part of the study were mainly qualitative in nature, as the criteria for determining if a burner was satisfactory were mostly visual. The flame from the burner was observed for color, steadiness, and size, among other qualities. Thus, a series of photographs of the various burners operating on liquid fuel will now be presented as that will best inform about the success of each burner design.

4.1.1 Custom Burner Results

The custom burner was able to produce a blue premixed flame at outputs over 1 kW. However, this design required some amount of careful observation and adjustments while operating. The fuel and air flow rates needed to be constantly adjusted in order to keep the burner operating steadily. On occasion, the burner flame would simply extinguish, perhaps due to fuel vapor condensing in the delivery tubes leading from the square tube to the burner. Much of those tubes were not heated by the burner flame and were relatively cool, which could cause fuel vapor to condense reducing the amount of

fuel vapor reaching the burner to combust. The fuel condensation could even partially block the tubes. Heating the tubes with a torch or heat tape appeared to reduce this issue, but neither solution was practical outside of testing. Changing the geometry of the burner to have more of the delivery tubes heated by the burner flame would likely improve the reliability of the design. On other occasions, the burner would be able to produce a steady flame with little interference and few flow rate adjustments for long times, including up to an hour. The unreliable nature of this design was one of the greatest issues. When the burner was steadily operating, it operated well. Figure 4.1 shows the custom burner operating on kerosene fuel using the micropump for fuel delivery and the blower for air delivery at approximately 1 kW heat output.

Figure 4.1: Photograph of the custom burner operating on kerosene fuel at approximately 1 kW heat output.

The output of the burner was determined from the calibration plot of the micropump to determine the volumetric flow rate of the fuel, seen in Figure A.3, and a basic calculation:

$$q = \rho * V * \Delta h_c \tag{4.1}$$

where q is the power produced by the burner, ρ is the density of the fuel, V is the volumetric flow rate from the micropump calibration plot, and Δh_c is the heat of combustion of the fuel. The lower heating value was used for the heat of combustion since any produced water will be in the form of water vapor. The values of ρ and Δh_c are shown in Table 1.1.

Another issue of this burner design was that it required being in an upright orientation for proper operation. Gravity was required to keep the fuel properly flowing to the hot impingement plate ensuring rapid and complete vaporization. Also, buoyancy effects allowed the burner flame to most effectively heat the impingement plate. A design to be used in the field would likely require orientation-independent operation that was not realized in the current design.

This shows that it is possible to develop and build a burner of a design that will combust liquid fuels in a premixed fashion. Additional time and resources would likely yield a more reliable and flexible design, and possibly one of a smaller overall size.

4.1.2 Commercial Burner Results

While it was demonstrated in the previous section that a custom burner could be built to burn liquid fuels, this has been already accomplished in commercial products. The two commercial burners used in this study both were able to burn a number of liquid fuels in a premixed fashion. They were designed to be primarily used as a stove for camping and backpacking, but they also performed well for the requirements of this study.

As mentioned previously, the Brunton burner [14] was a simpler design that did not employ any preheating of the fuel, and relied solely on a hot impingement plate for fuel vaporization. Figure 4.2 shows the Brunton burner operating on kerosene fuel at approximately 1.4 kW heat output.

Figure 4.2: Photograph of the Brunton burner operating on kerosene fuel at approximately 1.4 kW heat output.

It may be difficult to see in the above photograph, but the flame produced by this burner was mostly blue and thus premixed. However, some yellow and orange coloring could be seen at the edges of the flame, possibly resulting from the unburned fuel and air mixture not being completely premixed. This can be seen in Figure 4.2 by carefully looking at the top-right section of the flame. Even though the flame was mostly premixed, the yellow and orange coloring indicated soot production, which would have a detrimental effect on any power generation system after prolonged operation.

This design also did not lend itself to be started electrically. The critical components of the burner that would need to be preheated before ignition are located inside the orange cup, without any easy way of accessing them. Directly heating the orange cup electrically, which would then conduct heat to the fuel line and nozzle, would not be practical due to the large mass of the cup, leading to a large amount of energy required to heat it.

The output of the Brunton burner was determined by weighing the fuel container before and after operation with a triple beam balance to determine the mass of fuel used from the recorded duration of operation. This yielded an average mass flow rate of fuel. Multiplying this mass flow rate with the heat of combustion of kerosene resulted in the burner power.

The MSR burner [15] utilized preheating of the liquid fuel before combusting, in addition to a hot impingement plate. It was chosen over the Brunton burner for further experimentation due to its more sophisticated design, which produced a more fully premixed flame. Also, its design lent itself to electrical preheating more readily than the Brunton burner. Figure 4.3 shows the MSR burner operating on kerosene fuel at an output of approximately 2.4 kW. The burner output was determined by the same method as the Brunton burner.

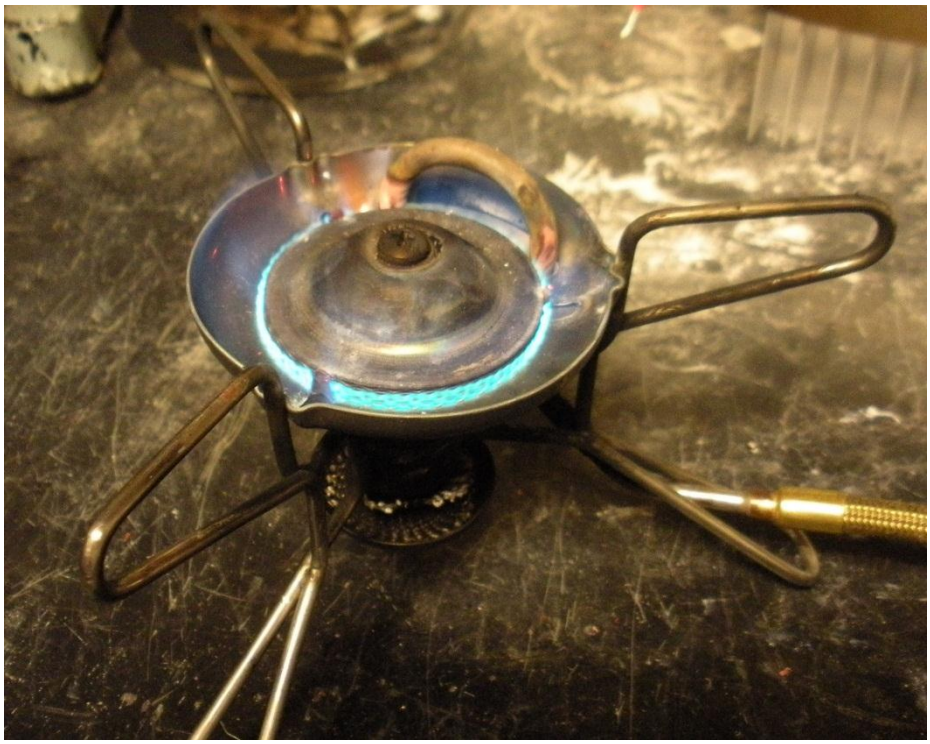

Figure 4.3: Photograph of the MSR burner operating on kerosene fuel at approximately 2.4 kW heat output.

The flame produced by this burner was completely blue in color, which indicated that the fuel and air mixture was fully premixed before combusting. This flame would not produce significant amounts of soot, and therefore this burner could be run for extended periods of time without detriment to an overall system. In addition, it should be noted that the design of this burner was well suited for this study due to its burner cup effectively directing the majority of the produced heat upward, which would then pass through the heat exchanger sitting on top of it.

4.2 THERMOELECTRIC MODULE PERFORMANCE RESULTS

Prior to incorporating thermoelectric generator modules into a complete burner and heat exchanger system, the performance of these modules under the controlled conditions described in Chapter 3.3 were examined. The results from this

experimentation, such as determining an optimal resistive load, could then be used to optimize the overall system.

Figure 4.4 shows the power output of a single thermoelectric module plotted as a function of applied load to the module for various temperature differences between the hot and cold sides of the module.

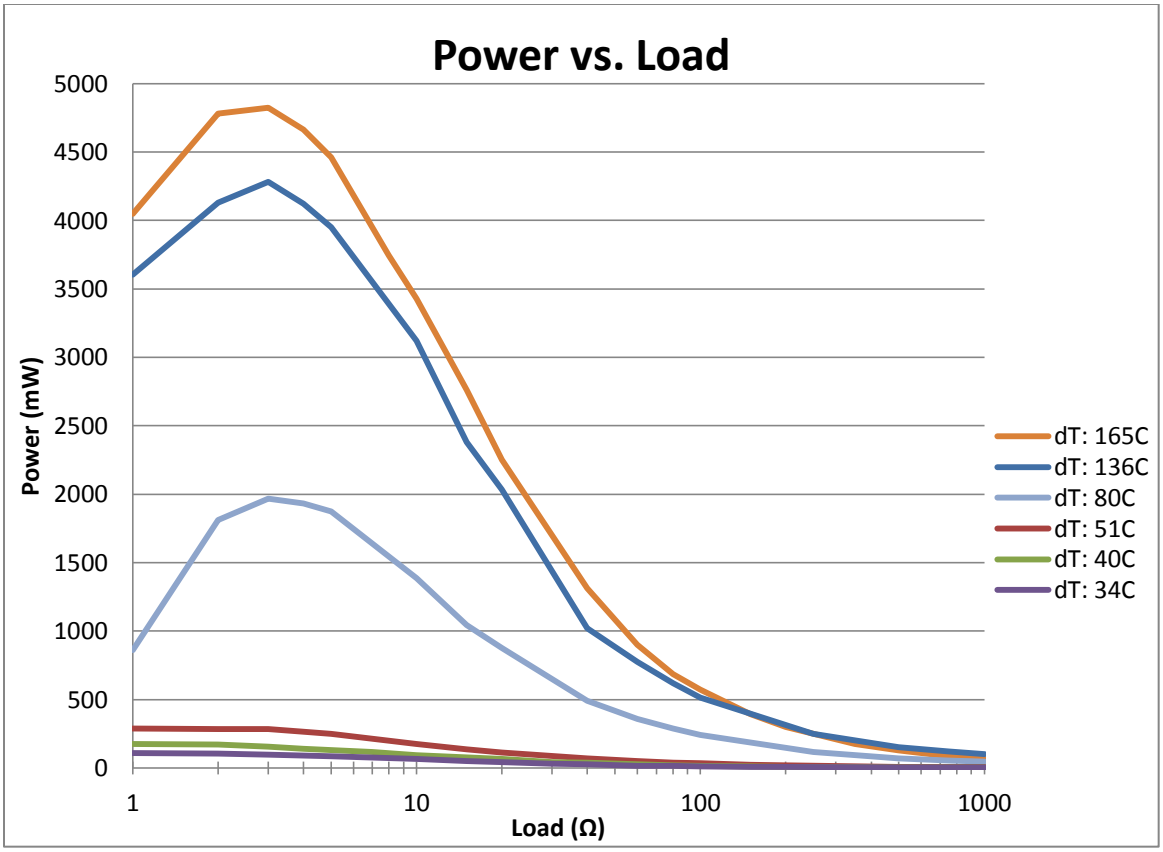

Figure 4.4: Plot of power output of a single thermoelectric module v. load at different temperature differences between the hot and cold sides of the module.

It can easily be seen that a higher temperature difference between the two sides of the thermoelectric module yields a higher power output for all loads. This agrees with thermoelectric theory, and is also intuitive.

The power output peaks at approximately 3 ohms for the larger temperature differences, and is approximately steady to 3 ohms followed by a drop-off for the smaller differences. This influence of resistive load on power output is significant. It should be noted that the load is plotted on a logarithmic scale to resolve the power peak. This peak would be much sharper on a linear axis. Thus, to get the maximum power output from these thermoelectric modules, the resistance of whatever it is powering should be approximately 3 ohms, and this is true for all module operating conditions.

Very little deviation from this optimal load will greatly reduce power output. For example, a load of 20 ohms will cut the available power by more than half. This adds a great deal of complexity to developing any system using a thermoelectric power source, as not only will the thermoelectrics have to be designed to provide sufficient power to a device, but the device must also be designed such that its electrical resistance will allow it to receive the greatest amount of power from the modules.

Figure 4.5 shows the power output at a 3 ohm load of a single thermoelectric module with its open circuit voltage plotted as a function of the temperature difference, or delta T, between the hot and cold sides.

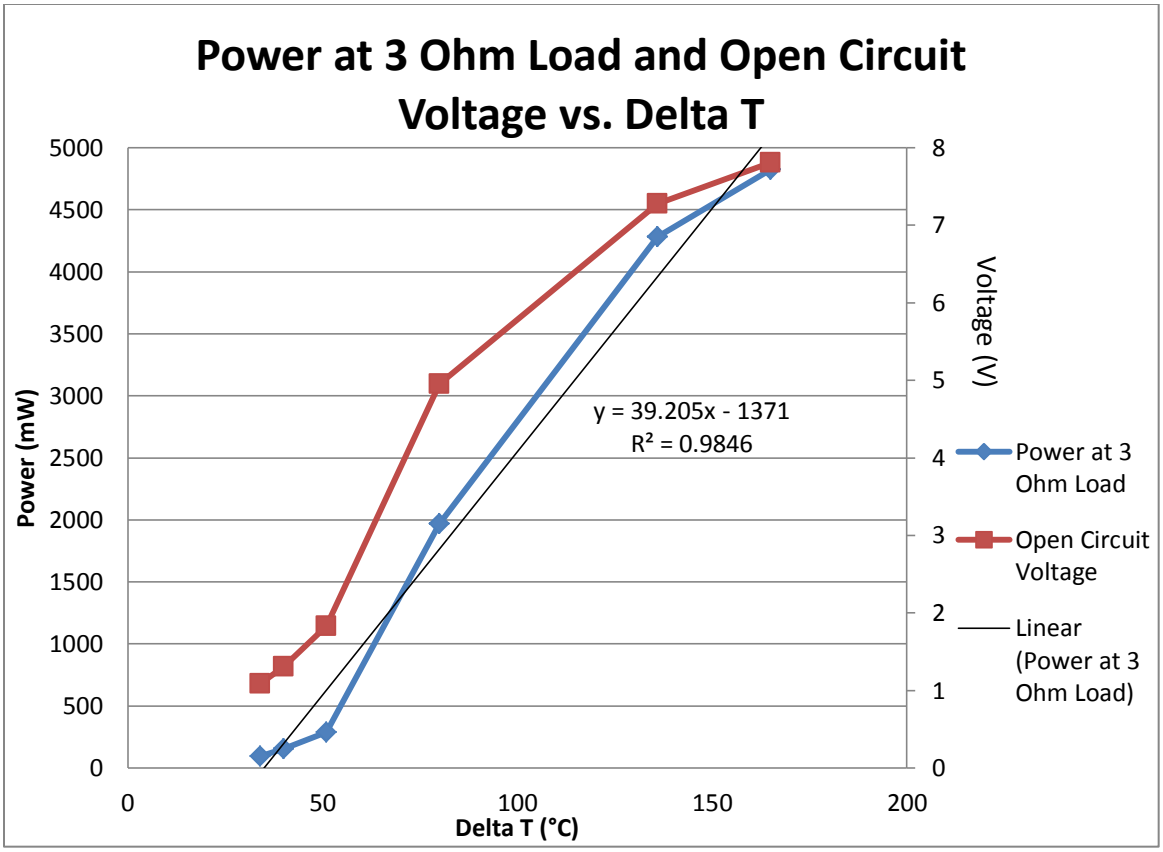

Figure 4.5: Plot of power output of a single thermoelectric module at a 3 ohm load and open circuit voltage v. delta T.

It can be seen that the power output and open circuit voltage follow the same trends as a function of delta T. This is significant because it is much easier to measure the voltage of a thermoelectric module not connected to a circuit than both the voltage and current of a module already in a circuit. So, for a basic qualitative analysis, the open circuit voltage of a module can be measured to indicate if a change in operating conditions will increase or decrease its maximum potential power output.

Aside from very low delta T values, the trend between power output and delta T is approximately linear. A linear curve fit line of the power data was included in the above figure, which has a very high R-squared value of almost 0.99 indicating an excellent fit.

Some of the nonlinearity could be due to experimental error. The temperatures were measured with K-type thermocouples, which have a standard limit of error of the greater of 2.2°C or 0.75% [22]. Also, the temperature of either side of the thermoelectric module might not have been spatially uniform. Finally, the resistance of the variable resistor attached in a circuit with the thermoelectric modules to provide a load could only be measured to the nearest ohm with available multimeters, so the applied load may not have been exactly 3 ohms. Even so, assuming a linear relationship between power and delta T at a 3 ohm load is adequate for a first-pass analysis.

4.3 Heat Exchanger Performance Results

4.3.1 Thermal Results

Since the heat exchanger did not have a circular cross-section but rather a square one, it was necessary to determine if the steady-state temperature profile of its outer wall was uniform across the width of it. A uniform temperature profile would simplify future experimentation as results would not be affected by measurement location across the heat exchanger's width. Figure 4.6 shows these results for the full length 16 inch long heat exchanger. Data were taken with and without attached thermoelectric modules. These results can be readily extended to the shorter heat exchangers as well. It should also be noted that the only cooling mechanism on the exterior of the heat exchangers was natural convection. These results will likely change in the presence of any other cooling mechanisms such as forced air cooling or liquid cooling.

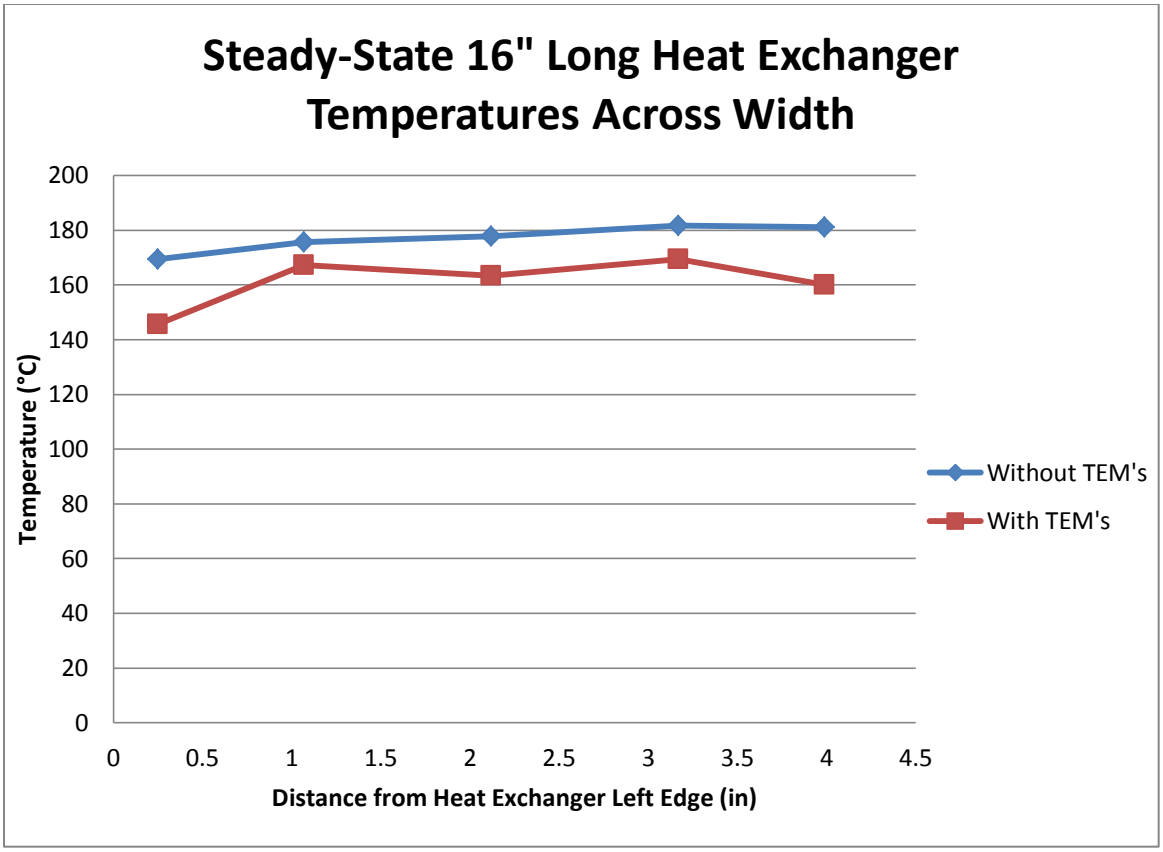

Figure 4.6: Plot of steady state temperature v. distance from the left edge of the 16 inch long heat exchanger across its width for cases with and without attached thermoelectric modules.

It would be expected that if the temperature profile was not uniform, then the maximum temperature should occur at the midpoint of the width, since that is the point which is closest to the burner for a square cross-sectioned heat exchanger surrounding a circular burner. This is clearly not seen in these results. The case without attached thermoelectric modules show an extremely uniform temperature profile with the difference in temperature between the hottest and coolest points being only 12°C. Taken as a percentage of the maximum temperature in Kelvin, that is only a 2.6% difference.

The case with attached modules show a bit less linear temperature profile, but still one that is overall very uniform that doesn't have a temperature maximum at its midpoint. The maximum temperature difference is 24°C. Using the same percentage calculation as the case without thermoelectric modules yields a 5.4% difference. This is more significant, but it should be noted that the leftmost data point in this case is somewhat of an outlier. It is also the minimum temperature, which skews the overall temperature difference. The other four data points are much closer to each other. It also should be noted that the temperatures in this case are a bit lower than the case without attached thermoelectrics. This will be seen again in later results.

This experiment was performed again on the 11 inch long heat exchanger. This was to determine the repeatability of results across the difference length heat exchangers. Figure 4.7 presents the results.

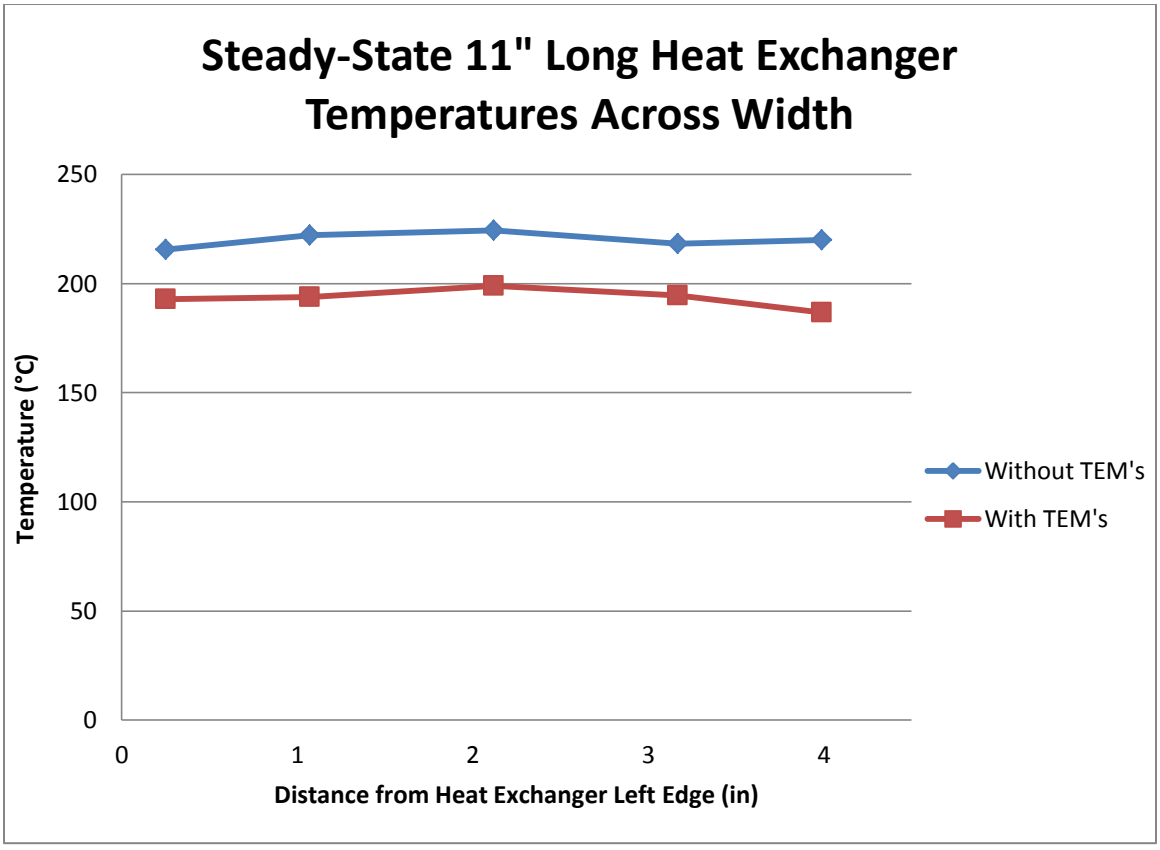

Figure 4.7: Plot of steady state temperature v. distance from the left edge of the 11 inch long heat exchanger across its width for cases with and without attached thermoelectric modules.

Once again, it is observed that the temperatures across the width of the heat exchanger are very uniform for cases both with and without attached thermoelectric modules. The maximum temperature difference for the case without attached modules is 9°C, yielding a 1.8% difference. For the case with attached thermoelectrics, the maximum difference is 12°C, yielding a 2.5% difference. Also, it is again seen that the case with attached modules yields lower overall temperatures. The actual temperatures should not be compared between the two heat exchangers since the data were taken at a different height on each heat exchanger: 8 inches from the bottom of the 16 inch long heat exchanger, and 3 inches from the bottom of the 11 inch long heat exchanger. However, the general

trends showing the uniformity of temperatures across a heat exchanger's width and that attaching thermoelectric modules lower those temperatures still hold.

The heat exchanger was positioned by hand over the burner, and lined up by eye. So, it may be the case that the heat exchanger was not completely centered over the burner. Being off-center by a couple millimeters is certainly possible. Figure 4.8 shows the effect on the steady state heat exchanger temperatures from deliberately positioning the heat exchanger approximately 1 centimeter off-center to the left. The temperature axis is zoomed in to more clearly show the results.

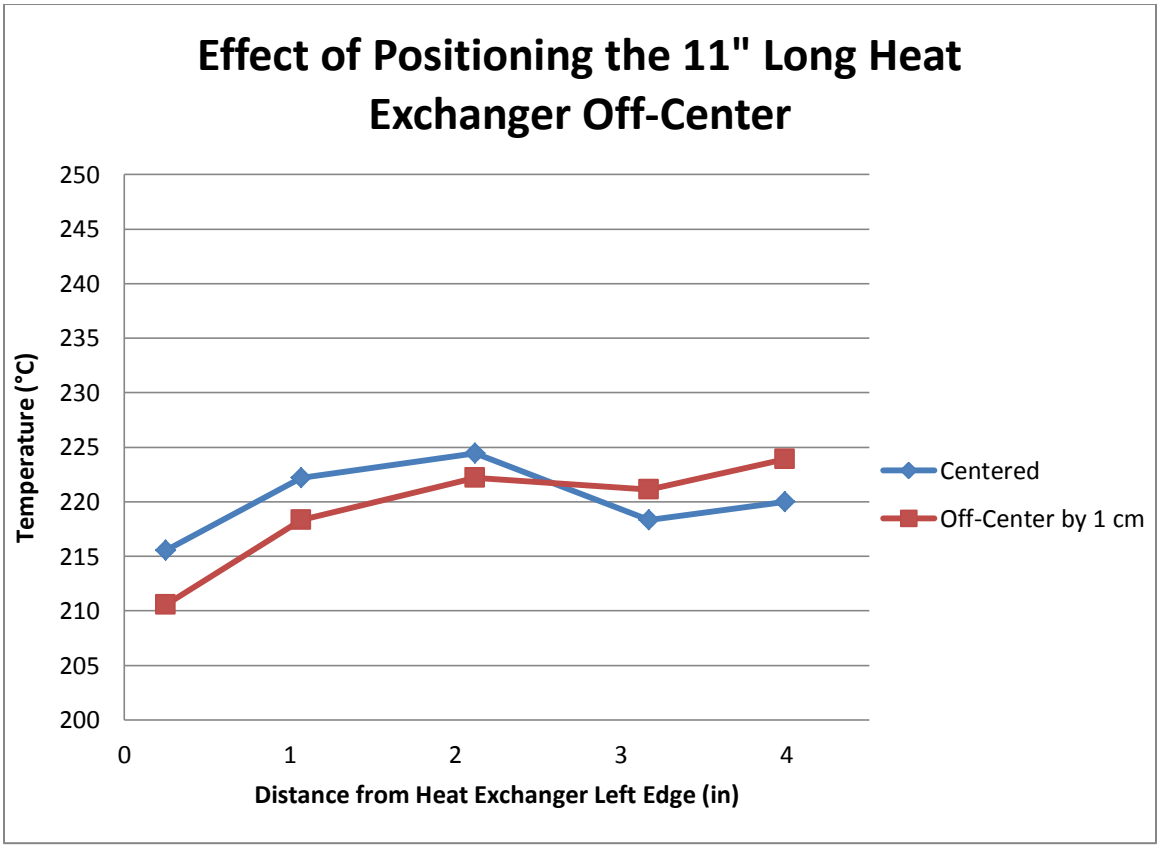

Figure 4.8: Plot of the effect on steady-state temperatures across the width of the 11 inch long heat exchanger without attached thermoelectric modules from deliberately positioning it 1 cm to the left.

It can be seen that the temperatures are reduced on the left side of the heat exchanger, and increased on the right side. By positioning the heat exchanger off-center to the left, the center of the burner flame was under its right side, raising the temperature on that side. The maximum difference between the centered and off-center cases is 5°C. It is unlikely that the heat exchanger was ever that far off-center during testing, but even a small deviation from center can have an effect on temperatures.

Also, as previously mentioned, the center of the heat exchanger was filled with ceramic fiber to route the hot exhaust gases through the finned area. However, this fiber may not have been packed fully uniformly resulting in complicated flow favoring one side of the heat exchanger. These are both possible sources of non-uniformity. Even so, it appears that the temperature of the heat exchanger is fairly uniform across its width, with and without attached thermoelectric modules.

While operating the burner with the heat exchanger on top of it, transient temperature data were recorded as the metal heated up. Only the temperatures at the top and bottom thermocouples were recorded to simplify the data collection process. These results for the 16 inch, 11 inch, and 5 inch long heat exchangers can be seen in Figures 4.9, 4.10, and 4.11 respectively. The results for the 16 inch long heat exchanger include data with and without attached thermoelectric modules, while the other two lengths only have data without attached thermoelectrics. These three figures were all plotted with the same time and temperature scales to best allow for easy comparison.

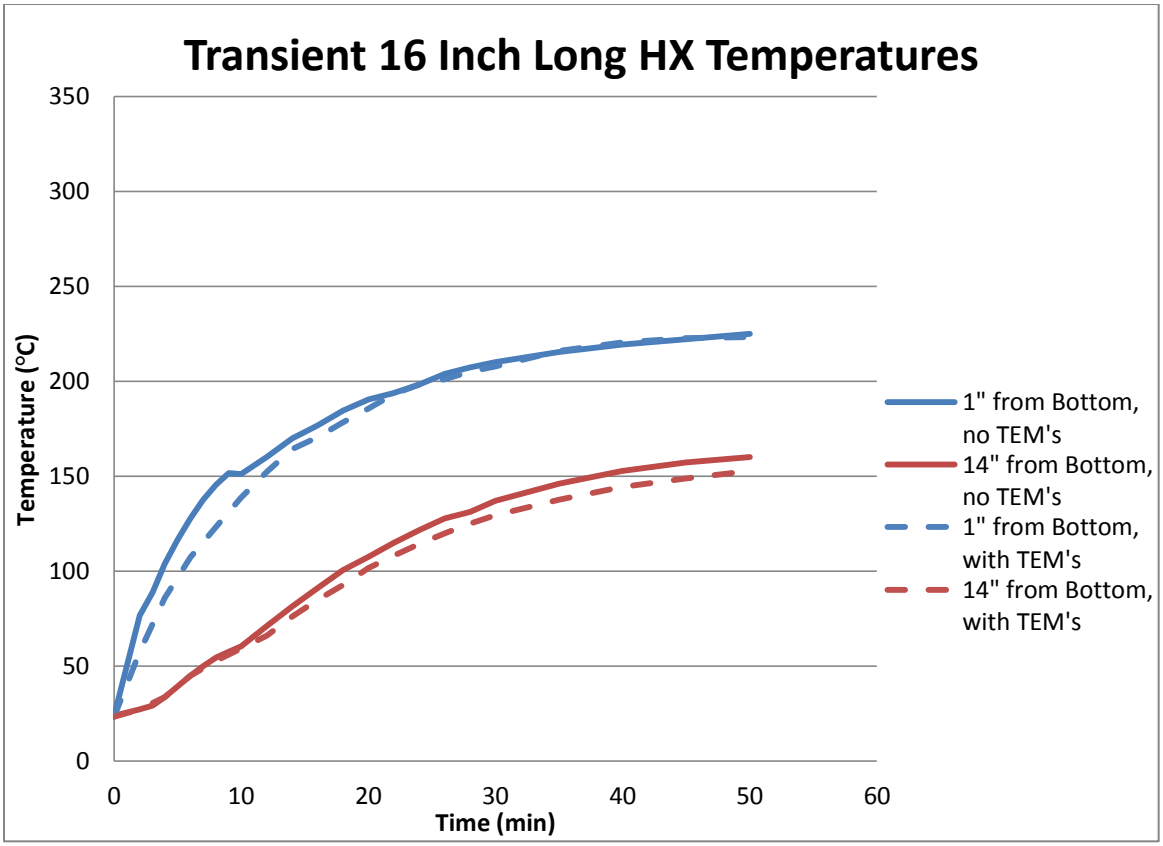

Figure 4.9: Plot of transient temperatures of the 16 inch long heat exchanger with and without attached thermoelectric modules taken at the top and bottom thermocouples.

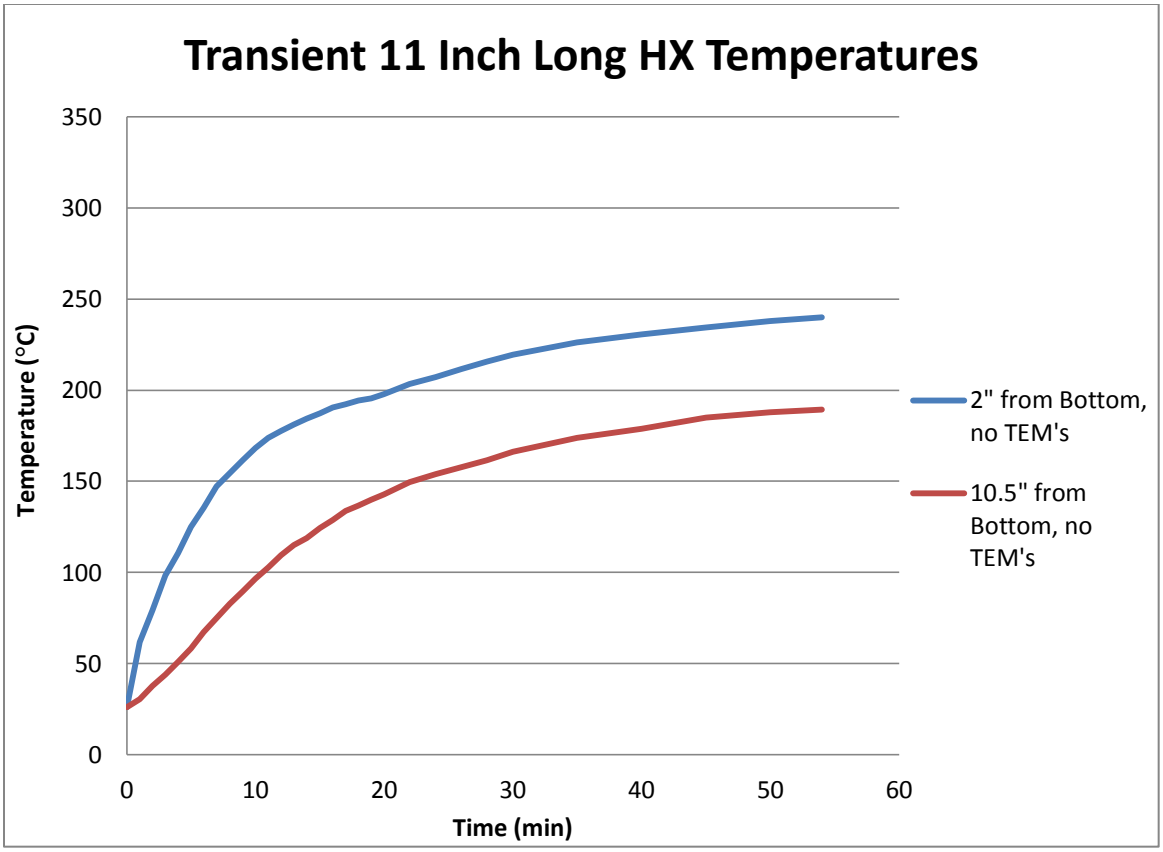

Figure 4.10: Plot of transient temperatures of the 11 inch long heat exchanger without attached thermoelectric modules taken at the top and bottom thermocouples.

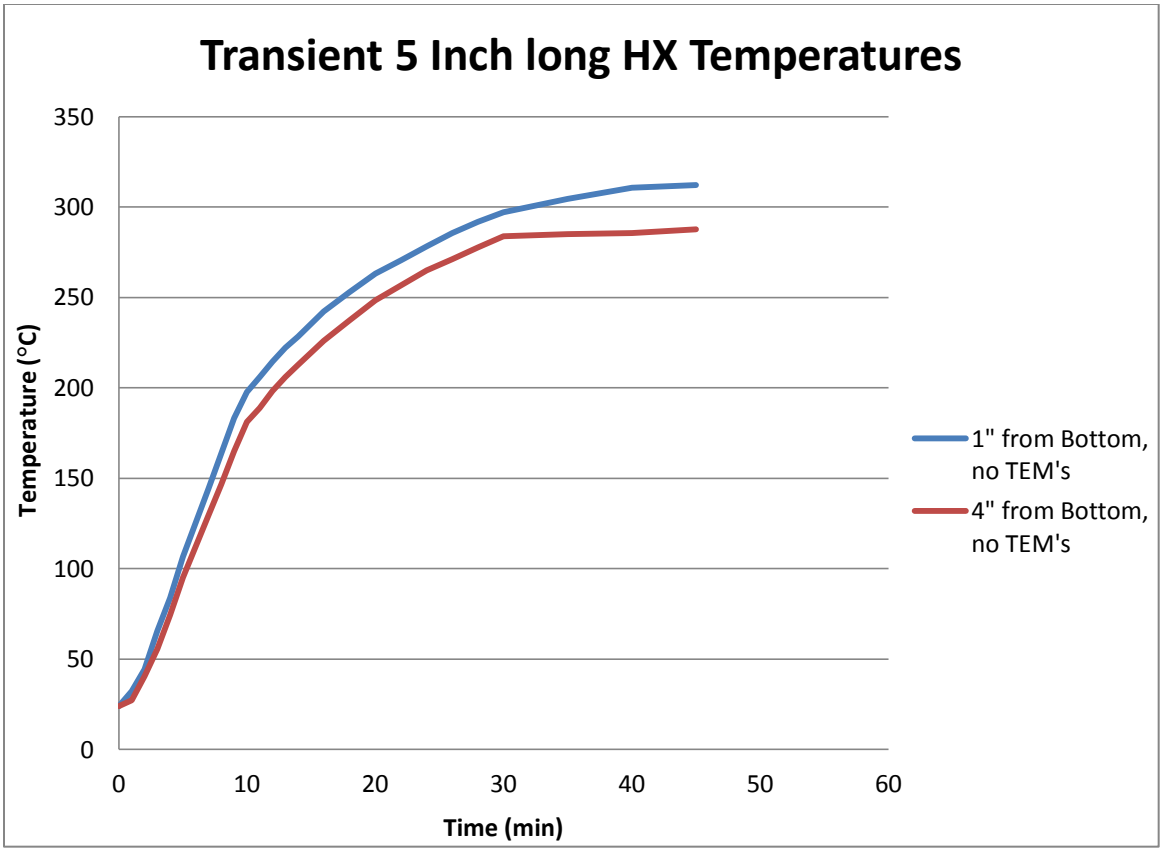

Figure 4.11: Plot of transient temperatures of the 5 inch long heat exchanger without attached thermoelectric modules taken at the top and bottom thermocouples.

It is seen from Figure 4.9 that the presence of attached thermoelectric modules does not affect the transient heat exchanger temperatures a great deal. They appear to lower the heat exchanger temperatures a small bit, likely due to the additional thermal mass, but the difference is so small that it could also be due to experimental error. For the 11 inch and 5 inch long heat exchangers, data were only collected without attached modules.

Steady-state was defined for these measurements as less than one degree Celsius change per minute, and that is when transient data stopped being recorded. It is interesting to note that for all three lengths of heat exchangers, steady-state was reached

within 10 minutes of each other. It was reached in about 50 minutes for the 16 inch long heat exchanger, about 55 minutes for the 11 inch long unit, and about 45 minutes for the 5 inch long unit. The time to reach steady-state did not show a clear trend with heat exchanger size. This means that for a field generator unit, the size of a heat exchanger used to capture the energy released from a burner will not greatly affect how much time it takes before the system reaches a steady electrical power output.

It is also seen that a smaller heat exchanger will yield higher overall metal temperatures. The 11 inch heat exchanger temperatures were slightly higher than the 16 inch unit, and the 5 inch heat exchanger temperatures were significantly higher than the other two lengths. It is desirable to have as much of the heat exchanger as possible near the maximum continuous operating temperature for the thermoelectric modules used in this study without significantly exceeding it. With a maximum allowable continuous operating temperature of 230°C for the thermoelectric modules, it appears that the 11 inch long heat exchanger is the optimal length out of the three in this respect. The temperatures of the 5 inch unit were so high that the thermoelectric modules may be damaged if attached to this heat exchanger when the burner system is running. It is expected, however, that efficiencies of future commercially available TEMs based on higher temperature materials such as skuteridites, for example, would benefit from the higher temperatures.

The next set of data show the steady-state temperature profiles of the different length heat exchangers along their height. In addition, the temperature profile of the exhaust gas as a function of distance from the burner is also presented. The 16 inch long and 11 inch long heat exchangers include data with and without attached thermoelectric modules, while the 5 inch long heat exchanger just has results without attached thermoelectrics. Figures 4.12, 4.13, and 4.14 present the data for the 16 inch long, 11

inch long, and 5 inch long heat exchangers respectively. The first data point closest to the flame was taken about one inch from the flame leading to the plotted temperatures that are significantly lower than the expected flame temperature.

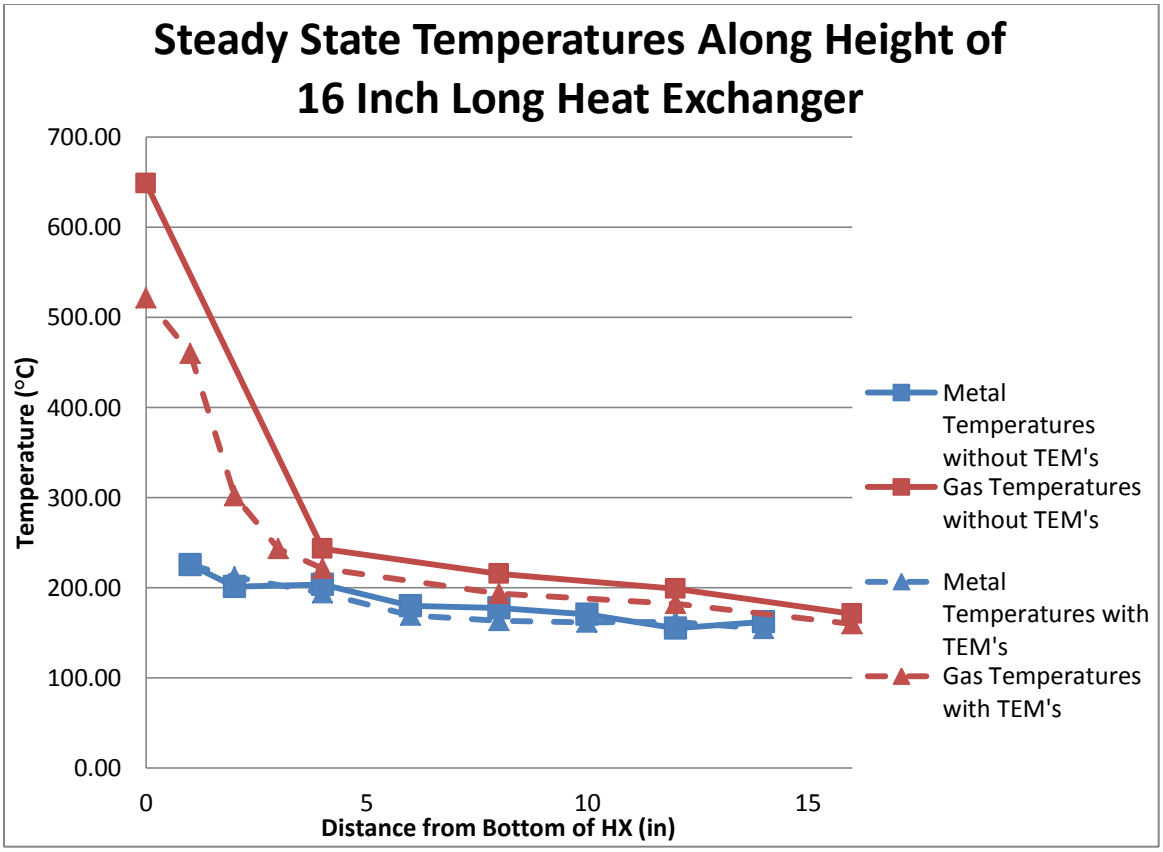

Figure 4.12: Plot of steady state metal and gas temperatures for the 16 inch long heat exchanger with and without attached thermoelectric modules v. distance from the bottom of the heat exchanger.

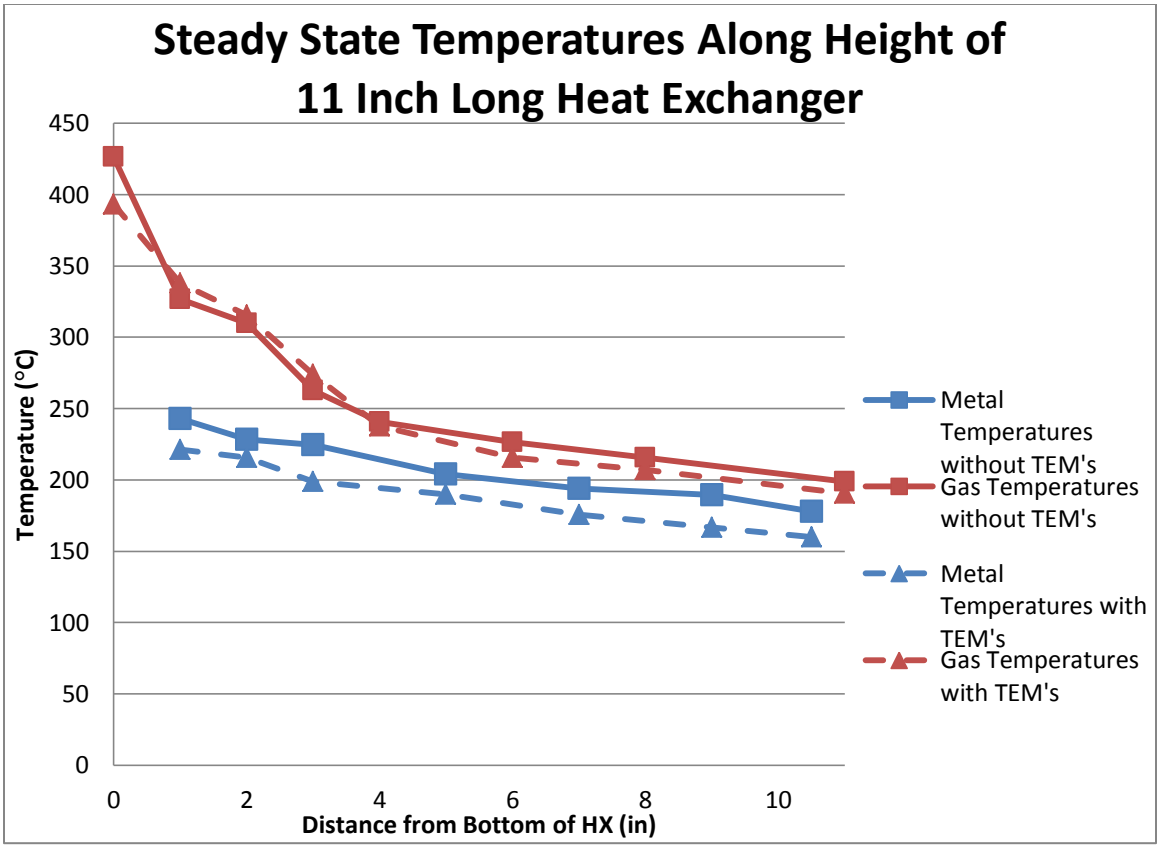

Figure 4.13: Plot of steady state metal and gas temperatures for the 11 inch long heat exchanger with and without attached thermoelectric modules v. distance from the bottom of the heat exchanger.

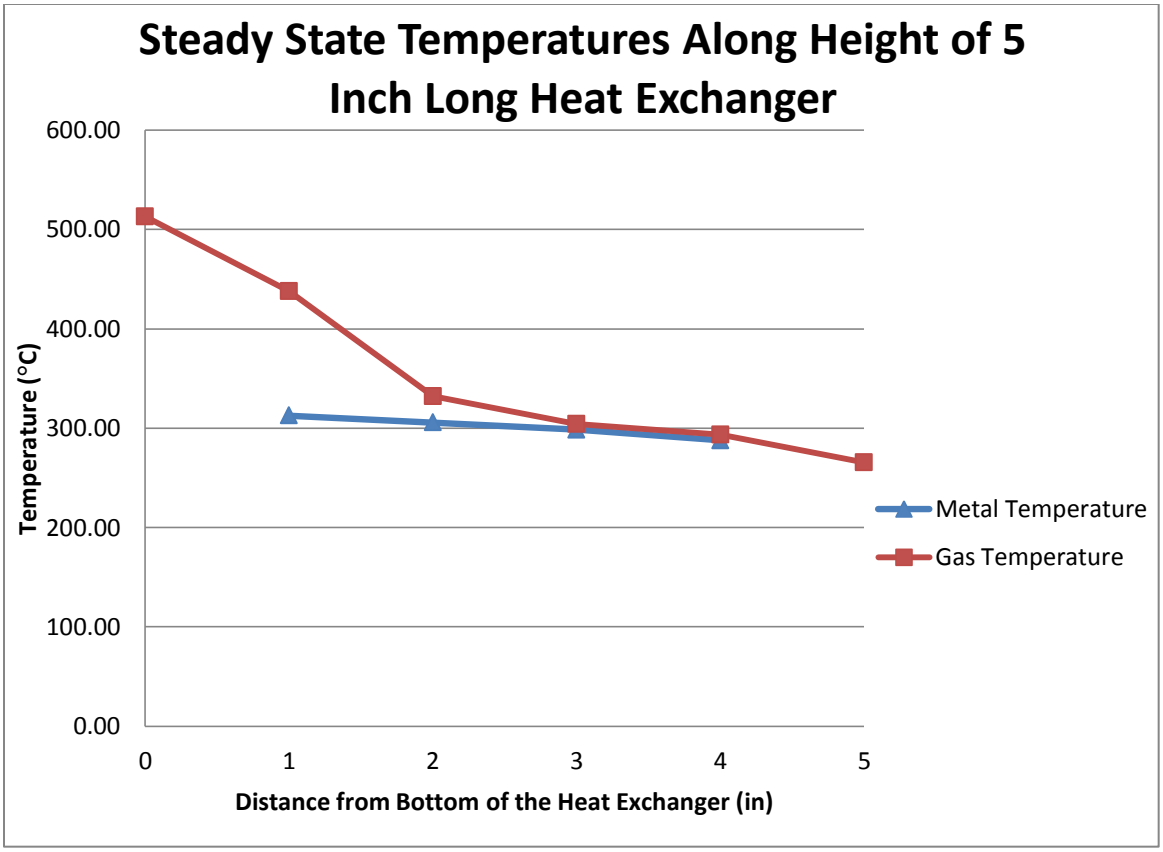

Figure 4.14: Plot of steady state metal and gas temperatures for the 5 inch long heat exchanger without attached thermoelectric modules v. distance from the bottom of the heat exchanger.

As can be seen in Figure 4.12, the presence of attached thermoelectric modules again does not greatly affect the metal temperatures of the 16 inch long heat exchanger, and even appears to lower it a bit. The metal temperatures of the 11 inch long heat exchanger, seen in Figure 4.13, show more of a difference between the cases with and without attached modules, but the general trend is the same; the case with attached modules has lower temperatures. The gas temperatures also appear to be reduced slightly for the cases with attached thermoelectric modules. However, this may be due to difficulty in measuring the gas temperatures, especially for the data points that are closest

to the burner. The thermocouple probe measuring the gas temperatures was held and positioned by hand, and a change distance of only a few millimeters could yield a change in temperature of up to 100°C when very close to the burner flame. While there is still a difference between the measurements with and without attached thermoelectrics for the gas data points that are further from the burner, it is not nearly as large as the first few points closest to the burner.

These plots show that the metal and gas quickly approach similar temperatures moving away from the bottom of the heat exchanger, which is where the burner is located. This is true for the heat exchangers of all three lengths. This indicates that the heat exchanger is very effective. It is able to quickly transfer the heat contained in the exhaust gas to the metal of the heat exchanger, which would then be transferred to attached thermoelectric modules. The gas temperature measurements were taken as far from the heat exchanger wall as possible, near the inner ceramic core. Measuring closer to the wall will likely show the wall and gas temperatures converging even sooner. The first gas temperature data point closest to the burner appears to vary significantly between the three different length heat exchangers ranging from about 400°C for the 11 inch unit with attached thermoelectrics to about 650°C for the 16 inch unit without attached thermoelectrics. Again, this is almost certainly due to experimental error. As mentioned previously, a slight change in distance of the thermocouple probe from the bottom of the heat exchanger can lead to a large change in temperature when very close to the burner flame. As the probe was hand-held, there very well may have been slight variations in positioning of the probe. Therefore, one shouldn't put much stock into the first gas temperature data point; it should just be used as a means to analyze trends within the same heat exchanger.

Figure 4.15 presents the metal temperature data for all three heat exchangers without attached thermoelectric modules on one plot. This data is also seen in Figures 4.12 through 4.14, but this is an easier way to make direct comparisons.

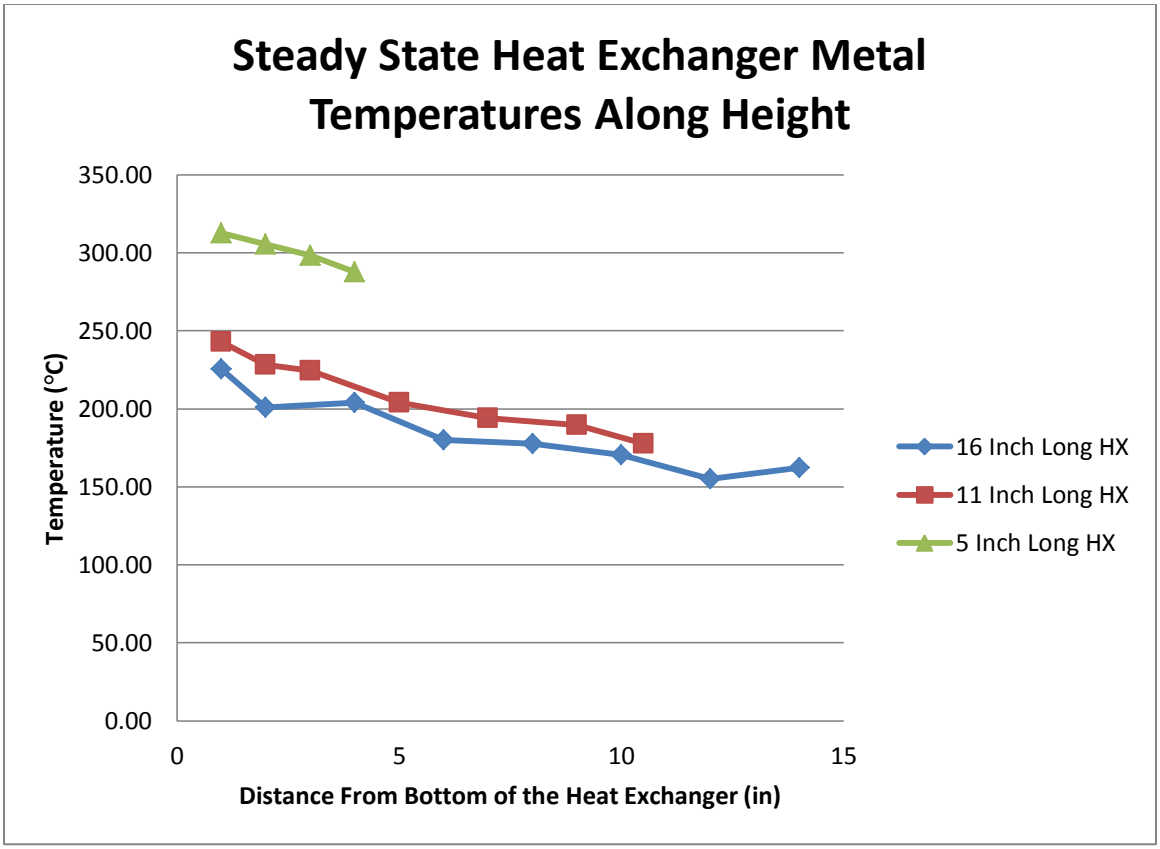

Figure 4.15: Plot of steady state metal temperatures for the three different length heat exchangers without attached thermoelectric modules v. distance from the bottom of the heat exchanger.

The general trend is that a shorter heat exchanger yields higher steady-state metal temperatures. The temperatures of the 5 inch long heat exchanger exceed the maximum allowable temperatures of the thermoelectric modules used in this study. So, attaching thermoelectrics to this shortest exchanger may lead to damage of the modules. The 11 inch long exchanger appears to provide the highest metal temperatures without exceeding

the module limits. However, this doesn't take into account any cooling that may be used on the cold side of the thermoelectrics in order to get the best possible performance out of them. Simply attaching the modules have not greatly affected heat exchanger surface temperatures, but adding cooling could significantly lower these temperatures.

4.3.2 Electricity Generation Results

Figure 4.16 presents transient temperature and open circuit voltage data for the 16 inch long heat exchanger. The thermocouple measuring the temperature of the outer wall of the heat exchanger and the attached thermoelectric modules were both at the same height on the heat exchanger.

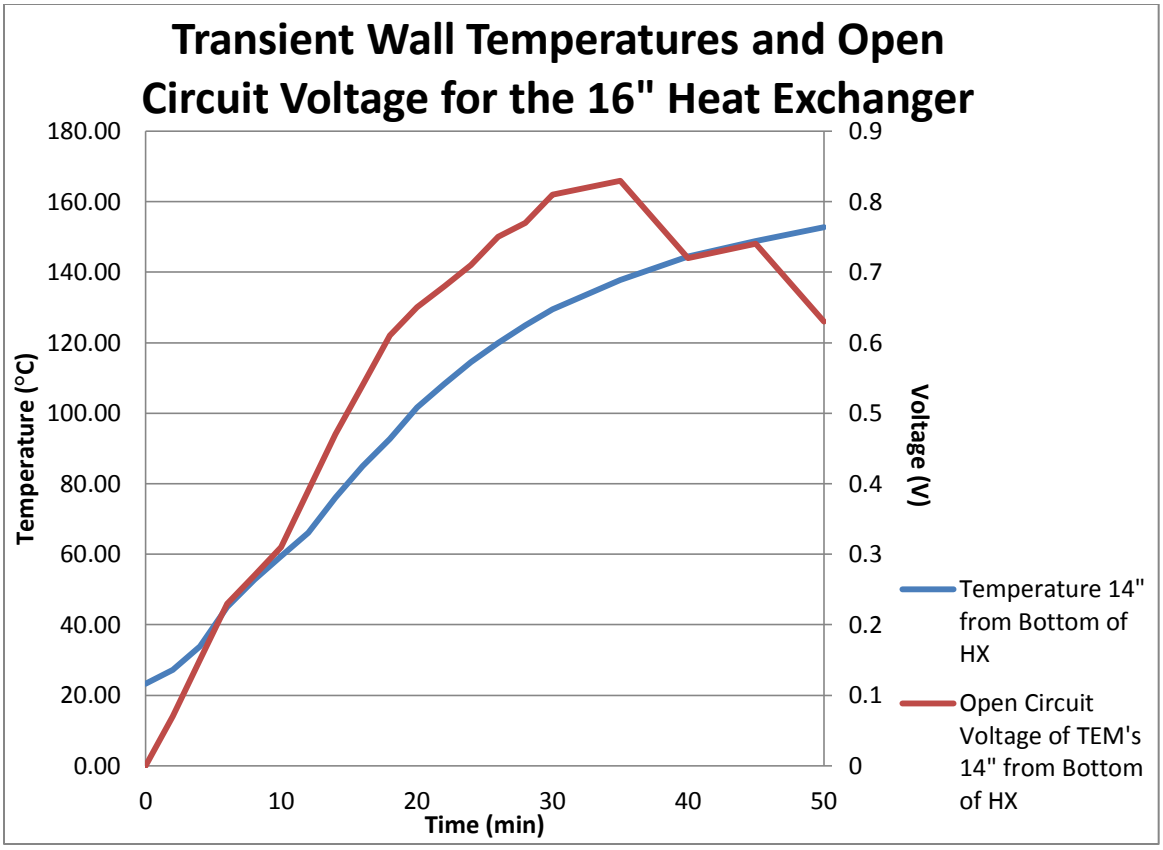

Figure 4.16: Plot of transient temperature and open circuit voltage data, both taken at the same height on the 16 inch long heat exchanger.

The temperature increases as expected, and reaches steady-state in approximately 50 minutes. This matches results from previous testing. The open circuit voltage also begins increasing with the temperature, but reaches a maximum value at about 30 minutes into the experiment. Afterwards, the voltage begins to drop. Since it was determined from Figure 4.5 that the thermoelectric module open circuit voltage follows a similar trend to its power output, this indicates that the power also reached a maximum followed by a drop during testing.

This is likely due to the thermoelectric module's cold side lagging behind its hot side in heating up. The hot side was in good thermal contact with the heat exchanger,

aided by an application of heat sink compound. So, the hot side was very close in temperature to the metal temperature of the heat exchanger. The heat had to be conducted through the thermoelectric module, which has a much lower thermal conductivity compared to the aluminum making up the heat exchanger. The thermal conductivity of the thermoelectric module is about 2 W/m*K [19], while a typical value for the thermal conductivity of aluminum is 237 W/m*K [23]. Thus, the cold side will not begin to heat up as quickly as the hot side leading to a larger temperature difference and therefore a larger open circuit voltage. After some time, the cold side does start to heat up and its temperature begins to approach the hot side temperature leading to the degradation in performance. A cooling solution for the cold side of the thermoelectric module will prevent this performance degradation from occurring, and will also improve overall power output by lowering the cold side temperature.

Table 4.1 presents data relating the steady-state temperatures of various thermoelectric modules attached to the 16 inch long heat exchanger at different heights with their open circuit voltage. The top five rows each consisted of two bare modules connected in series. The bottom row consisted of one bare module and one module with a CPU-style heat sink attached to its cold side connected in series.

Distance From Bottom of Heat Exchanger (in)	Cold Side Temperature (°C)	Hot Side Temperature (°C)	Delta T (°C)	Open Circuit Voltage (V)	
14	267	310.00	43.00	0.63	
12	282	324	42.00	0.79	
10	287	323	36.00	0.86	
6	300	337	37.00	0.86	
4	337	381	44.00	0.85	
1.5	N/A	N/A	N/A	2.72	*Both modules connected in series
1.5	385	425.8	40.80	0.41	*Bare module only
1.5	312	425.8	113.80	2.28	*Module with heat sink only

Table 4.1: Steady-state temperature and open circuit voltage data for thermoelectric modules attached at different heights on the 16 inch long heat exchanger.

As expected, both the hot side and cold side temperatures increase moving towards the bottom of the heat exchanger, which is where the burner is located. However, except for the module with the attached heat sink, the steady-state temperature differences between the hot side and cold side of the modules remain fairly constant with varying height on the heat exchanger. Accordingly, the open circuit voltages, and therefore the power output, also remain fairly constant.

The module with the attached heat sink is the only one that counters this trend. The cold side temperature is significantly lower than the other module at the same height but without the attached heat sink. As such, the temperature difference is much higher than any of the other modules, leading to a much higher open circuit voltage. It is clear that cold side cooling is necessary to achieve the best possible performance out of these thermoelectric modules.

This knowledge was implemented in testing with the 5 inch and 11 inch long heat exchangers. The thermoelectric modules were attached to the heat exchangers, and a

long heat sink was attached to their cold side. This setup was shown in Figure 2.14 for the 5 inch heat exchanger. A 3 ohm resistor was attached to the modules to determine their maximum power output. The open circuit voltage, and the power determined from the loaded voltage and current were measured. The average hot side and cold side temperatures were also calculated. The measured temperatures used to calculate these average temperatures are presented in Appendix D. The presence of the long heat sink made it difficult to measure anything more precise than average temperatures of the heat exchanger and heat sink. In addition, data were taken with and without active cooling of the heat sink. For this experiment, active cooling consisted of a blower blowing air over the heat sink, which was seen in Figure 2.15. The results for the 5 inch long heat exchanger can be seen in Table 4.2, and the results for the 11 inch long heat exchanger can be seen in Table 4.3.

	Open Circuit Voltage (V)	Voltage with Load (V)	Current with Load (A)	Power (W)	Avg. Hot side Temperature (°C)	Avg. Cold Side Temperature (°C)	Delta T
Upper TEM Passive Cooling	2.38	1.22	0.36	0.44	219	134	85
Lower TEM Passive Cooling	2.14	1.08	0.32	0.35	219	134	85
Upper TEM Active Cooling	5.27	2.98	0.78	2.32	163	56	107
Lower TEM Active Cooling	4.77	2.58	0.72	1.86	163	56	107

Table 4.2: Experimental results for the 5 inch long heat exchanger with attached thermoelectric modules and cold side cooling.

One module was attached towards the top of the 5 inch long heat exchanger and one was attached towards the bottom. This was done to see a general trend of performance across the entire heat exchanger's height. The top module appears to perform a bit better, but there isn't a great difference. Actively cooling the cold side of the modules improved performance greatly. While it did lower the hot side temperature, it also lowered the cold side temperature by a greater amount resulting in a larger temperature difference, and therefore higher power output. The downside of employing active cooling is that the blower requires power to operate, decreasing the net power produced by the system. The blower was measured to use about 8 W of electricity at full power. Each face of this heat exchanger can fit about 4 modules, and assuming an average of the power output for the upper and lower actively cooled modules, each side

could produce a bit over 8 W of electricity. Thus, with the blower used for this experiment, there wouldn't be any significant net power output for this setup using active cooling. A more efficient active cooling system would need to be developed. Passive cooling relying solely on natural convection, on the other hand, would produce about 1.58 W per side of the heat exchanger resulting in a total output of 6.32 W.

	Open Circuit Voltage (V)	Voltage with Load (V)	Current with Load (A)	Power (W)	Avg. Hot side Temperature (°C)	Avg. Cold Side Temperature (°C)	Delta T
Upper TEM Passive Cooling	1.65	0.76	0.26	0.20	210	139	71
Middle TEM Passive Cooling	1.64	0.75	0.26	0.20	210	139	71
Lower TEM Passive Cooling	2.65	1.26	0.44	0.55	210	139	71
Upper TEM Active Cooling	3.07	1.45	0.51	0.74	163	53	110
Middle TEM Active Cooling	3.18	1.51	0.53	0.80	163	53	110
Lower TEM Active Cooling	4.97	2.4	0.86	2.06	163	53	110

Table 4.3: Experimental results for the 11 inch long heat exchanger with attached thermoelectric modules and cold side cooling.

For the 11 inch heat exchanger, three thermoelectric modules were used: one towards the top of the heat exchanger, one towards the middle, and one at the bottom. Again, this was done to deduce an average performance across the heat exchanger's height. The upper and middle modules performed similarly, and the lower module showed the best performance. Adding active cooling improved the performance of all the modules by approximately a factor of four. Once again, the active cooling cooled both the hot and cold sides of the modules, but lowered the cold side temperature by a greater amount resulting in a larger temperature difference, resulting in more power output. Averaging out the power output of the three attached modules results in about 0.32 W produced per module when passively cooled, and about 1.2 W per module with active cooling. Each side of this longer heat exchanger can fit about 10 modules resulting in 3.2 W produced with passive cooling, or 12.8 W for the entire heat exchanger. Active cooling results in 12 W produced per face, which after subtracting the 8 W used by the blower leaves 4 W net, or 16 W net for the entire heat exchanger. The active cooling system can likely be greatly improved yielding better net performance. The power output data from Tables 4.2 and 4.3 are summarized in Figure 4.17.

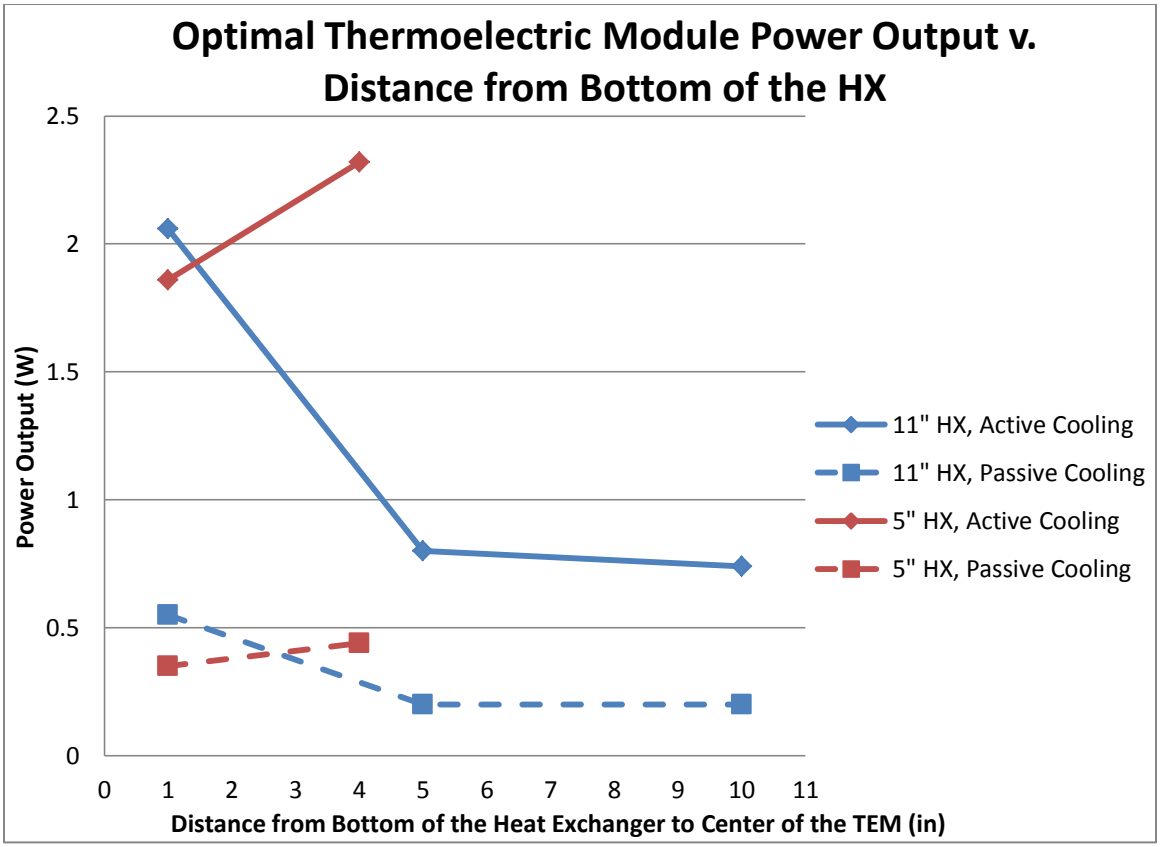

Figure 4.17: Plot of optimal thermoelectric module power output v. distance from the bottom of the heat exchanger, using both active and passive cooling.

Some of the variation seen in the above plot for a particular length heat exchanger and type of cooling can possibly be due to differing efficiencies between individual thermoelectric modules. Some modules may have been used more often and at more extreme conditions than others during testing, and that use could possibly affect their efficiency. Also, while it was attempted to make the contact between the modules and the heat sink and heat exchanger the same for all modules, there may have been some differences affecting contact resistances, and therefore heat transfer.

4.4 Balance of Plant Analysis

There aren't very many sources of parasitic loss associated with this system, and each one of the sources tends to result in a rather small loss. However, as the thermoelectric modules do not produce a great deal of electrical power, the parasitic losses can be significant.

The literature for the micropump used for fuel delivery to the custom burner states that it requires about 200 mW for operation [12]. The controller used for testing requires about 3.75 W for operation, but a microchip controller is available that only requires about 150 mW [20]. A final unit would likely use the microchip controller. The fuel delivery system for the commercial burners did not require additional electricity. They operated through the pressurization of a fuel bottle, and therefore are not a parasitic load. The method to determine the fuel delivery rate in the commercial burners was described in Chapter 4.1.2.

The blower that was used for air delivery to the custom burner was measured to use a maximum of about 8 W of power. However, the custom burner required a lower air flow rate than what the blower could provide. In general, the blower operated at about one quarter of its maximum output, which requires about 2 W of power. The commercial burners did not require a separate air delivery system.

The same blower was also used to actively cool the heat sinks attached to the cold side of the thermoelectric modules. In this case, the blower was operated at its maximum output requiring 8 W of power, and a separate blower would be required for each of the four sides of the heat exchanger. This could very likely be improved.

The starting system for the custom burner used the ceramic heater for preheating, while the MSR commercial burner used both the ceramic heater and cartridge heater. As these devices only needed to be operated for a short period of time at the beginning of

running the system, they would not be a parasitic load on the system during steady-state operation. There would just need to be sufficient power in an attached electrical storage device to operate the start-up systems. The same can be said for a source of initial ignition, be it a glow-plug, a sparker, or other device.

The parasitic losses associated with operation of this burner system are summarized in Table 4.4.

	Custom Burner	Commercial Burner
Fuel Delivery	350 mW	N/A
Air Delivery	2 W	N/A
Active Cooling	32 W	32 W
Total:	34.4 W	32 W

Table 4.4: Chart summarizing the parasitic load of the custom burner and commercial burner systems.

The losses from active cooling dominate the parasitic loads. This is a key area of possible improvement.

4.5 UEGO AND HEAT EXCHANGER EFFICIENCY RESULTS

The UEGO sensor measured a fuel to air equivalence ratio of about 1.05 (slightly rich) for several experiments using the MSR burner, which is very close to stoichiometric. These data allowed a heat exchanger energy balance analysis to be performed. The details of this calculation can be seen in Appendix B. The efficiencies were calculated for the case without attached thermoelectric modules. The presence of attached modules did not greatly affect the temperature of the gas exiting the heat exchanger, and therefore would not greatly affect these heat exchanger efficiency

calculations. Of course the efficiency of electricity generation would be a strong function of the number of thermoelectric modules and their placement.

These calculations show that the 16 inch long heat exchanger was 94.4% efficient. Or, it was able to extract 94.4% of the energy released from the combustion of the liquid fuel. The heat exchanger efficiency was defined to be the amount of energy extracted by the heat exchanger divided by the mass flow rate of the fuel times its lower heating value. The 11 inch heat exchanger was 93.4% efficient. Finally, the 5 inch heat exchanger was 90.7% efficient. It makes sense that a longer heat exchanger will be more efficient. All three lengths of heat exchangers performed excellently and were able to capture the vast majority of released energy. Figure 4.18 presents these efficiency results.

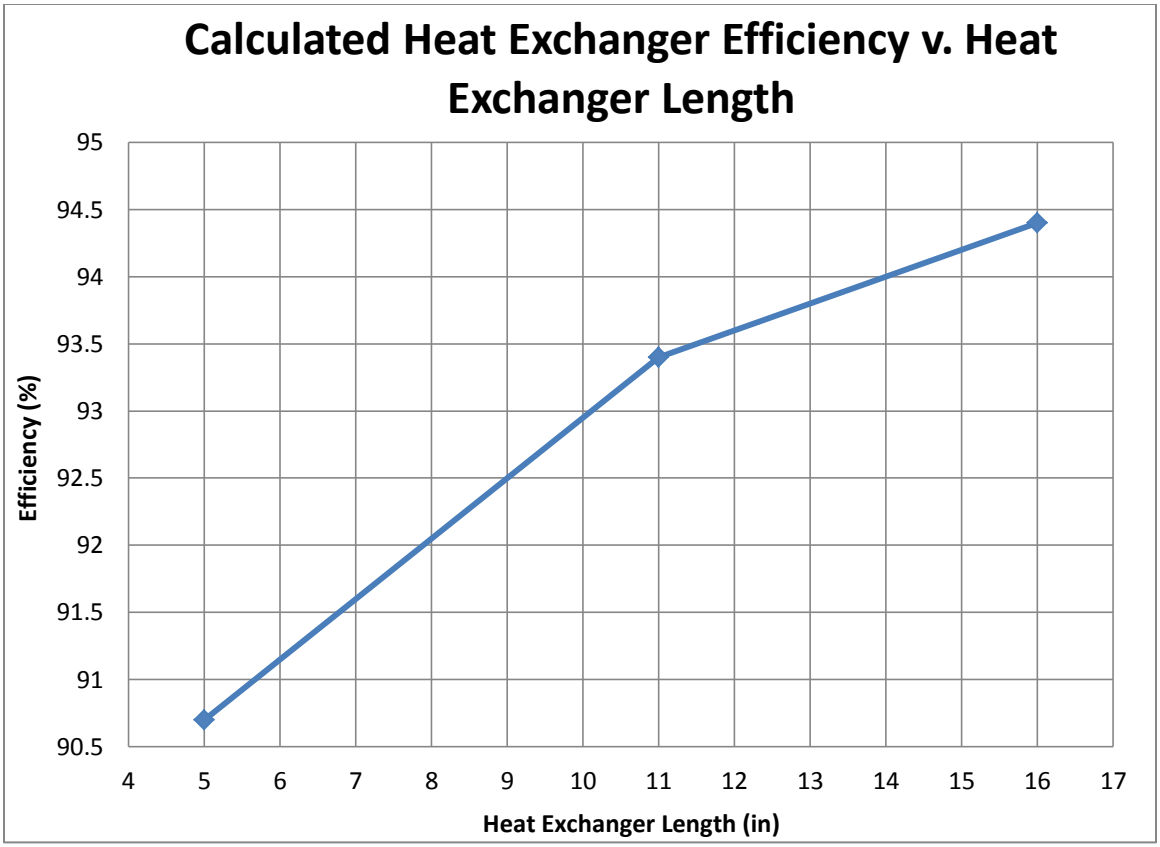

Figure 4.18: Plot of calculated heat exchanger efficiency v. heat exchanger length.

Chapter 5: Conclusions and Recommendations

5.1 Conclusions

5.1.1 Burner Design

A custom burner was designed and built to test the feasibility of combusting a liquid fuel in such a device to produce a blue premixed flame. It operated successfully on kerosene at outputs of over 1 kW. However, this design proved to be unreliable. The air and fuel flow rates were required to be carefully monitored and adjusted while the burner was operating. It is also likely that fuel vapor was condensing in fuel delivery tubes leading to the burner after initially vaporizing on the hot impingement plate. This would have the effect of reducing the amount of fuel reaching the burner due to loss from condensation, as well as partially blocking the delivery tubes resulting in less vapor able to pass through them. In addition, this design was required to be in an upright orientation for proper operation, which is not desirable for a unit to be used in the field.

Two liquid-fueled commercial burners were also tested that were both capable of outputs of over 1 kW. The Brunton burner was a simpler design that did not employ any method to preheat the incoming fuel before vaporization. The flame produced by this burner was mostly blue and thus premixed, but some yellow and orange coloring was seen towards the edges of the flame possibly due to some non-premixed combustion. This indicated that some soot was produced, which would have a detrimental effect on any power generation system after prolonged operation. This burner design also did not lend itself to be started electrically.

The MSR burner did utilize a method to preheat the fuel, as well as a hot impingement plate to fully vaporize it. It produced a completely blue flame indicating

that it was fully premixed. It was also easier to electrically start this burner. This burner was used for testing the heat exchanger and thermoelectric modules.

5.1.2 Thermoelectric Modules

The power output of the thermoelectric modules used in this study was very dependent on resistive load. An optimal load was determined to be 3 ohms. Deviating from that optimal load by even a relatively small amount had a large negative effect on power output. This adds a level of complexity to the design of any device to be powered by these modules; its electrical resistance must be close to 3 ohms in order to achieve the best possible performance. The power output had a linear relationship with the temperature difference between the hot and cold sides of a module. The open circuit voltage produced by a module followed a similar trend as power output, allowing one to simply measure voltage to qualitatively determine how various operating conditions would affect power output.

5.1.3 Heat Exchanger

It was determined that the temperature across a face of the square cross-sectioned heat exchanger was constant, allowing data to be collected at any location along the heat exchanger's width. However, the accuracy in centering the heat exchanger over the burner had a slight but noticeable effect on temperatures.

The length of the heat exchanger did not have a large effect on how long before the temperatures reached steady-state, indicating that the amount of time a field unit would require before producing a steady electrical power output was fairly independent from heat exchanger size. The heat exchanger proved to be very effective because the exhaust gas and metal temperatures rapidly approached similar temperatures downstream from the burner. A heat exchanger efficiency calculation showed that the 16, 11 and 5

inch long heat exchangers were about 94.4%, 93.4%, and 90.7% efficient respectively. The presence of attached thermoelectric modules lowered the heat exchanger temperatures slightly. A shorter heat exchanger yielded higher steady-state metal temperatures, which could exceed the maximum allowable continuous operation temperature of the thermoelectric modules that were used in this study.

Without cooling the cold side of the thermoelectric modules, power output peaked and then dropped while the system was in the process of reaching steady-state conditions, likely due to the cold side lagging behind its hot side in temperature while heating up. Cold side cooling remedied this issue and improved performance by increasing the temperature difference between the two sides of the thermoelectric module. Actively cooling the cold side with a blower and heat sink produced higher power output from the thermoelectric modules than using passive cooling employing just a heat sink because of a larger temperature difference between the two sides. For the 5 inch long heat exchanger, passive cooling produced an average hot side temperature of 219°C and an average cold side temperature of 134°C yielding a difference of 85°C. However, active cooling produced an average hot side temperature of 163°C and an average cold side temperature of 56°C yielding a difference of 107°C. For the 11 inch long heat exchanger, the average hot side temperature when using passive cooling was 210°C and the average cold side temperature was 139°C for a difference of 71°C. With active cooling, the average hot side temperature was 163°C and the average cold side temperature was 53°C for a difference of 110°C.

Active cooling introduced a parasitic load in the blower, but net power output was still higher than passive cooling for the 11 inch long heat exchanger. The system with the 11 inch long heat exchanger and active cooling could produce 16 W of net power output, but only 12.8 W with passive cooling. With the 5 inch long heat exchanger, about 6.3 W

could be generated with passive cooling, but there would be no net power generation with active cooling due to the large additional parasitic load. The blower parasitic load dominated all other parasitic loads in scale. Based on these results, it appears that an 11 inch long heat exchanger with the cold side of the attached thermoelectric modules actively cooled generates the most net electricity for a burner of similar output to the MSR burner, which is about 2 kW.

5.2 RECOMMENDATIONS

A deadline and funding issues prevented further work in this study. However, there is still much that can be further accomplished. The custom burner should be redesigned to make it more reliable. One way to accomplish this is to pass a larger percentage of the fuel delivery tubes through the burner flame to prevent vaporized fuel from condensing. In addition, the burner should be orientation-independent and more compact.

Further testing should be done to determine what if any effect the equivalence ratio of the burner has on performance of the heat exchanger and power output of the thermoelectric modules. It was difficult to alter the equivalence ratio of the MSR burner accurately and repeatably, so it might be best to test with the custom burner. Long term testing should also be completed to see if performance degrades over time. Possible sources of performance degradation could be a loss of heat exchanger effectiveness due to fouling from deposits released during combustion, and clogging of the burner fuel nozzle.

As the largest parasitic load on the system was the method to actively cool the cold side of the thermoelectric modules, work should be done to more efficiently accomplish this. One possible solution is to enclose the heat exchanger with a thin

sheathing that is open at the bottom and narrows to a smaller opening at the top. This would hopefully draw cool air over the heat sinks by entraining it in the exhaust gas flow out the top of the heat exchanger.

The heat exchanger design could likely be improved. The open center area of the heat exchanger used in this study was filled with ceramic as a makeshift solution to route hot gases through the finned area. A heat exchanger design without such a large open center through use of longer fins would not need the ceramic. In addition, reducing the weight of the heat exchanger should be investigated as some dimensions of its cross-section, seen in Figure 2.8, are likely larger than required. Also, additional heat exchanger lengths should be tested.

Much of the performance of the system was determined by the thermoelectric modules used in this study. It should be investigated if a more efficient and cost-effective thermoelectric generator, possibly with higher temperature limits, exists that could be used in this system.

Appendix A: Calibration Plots

A.1 Injector Calibration

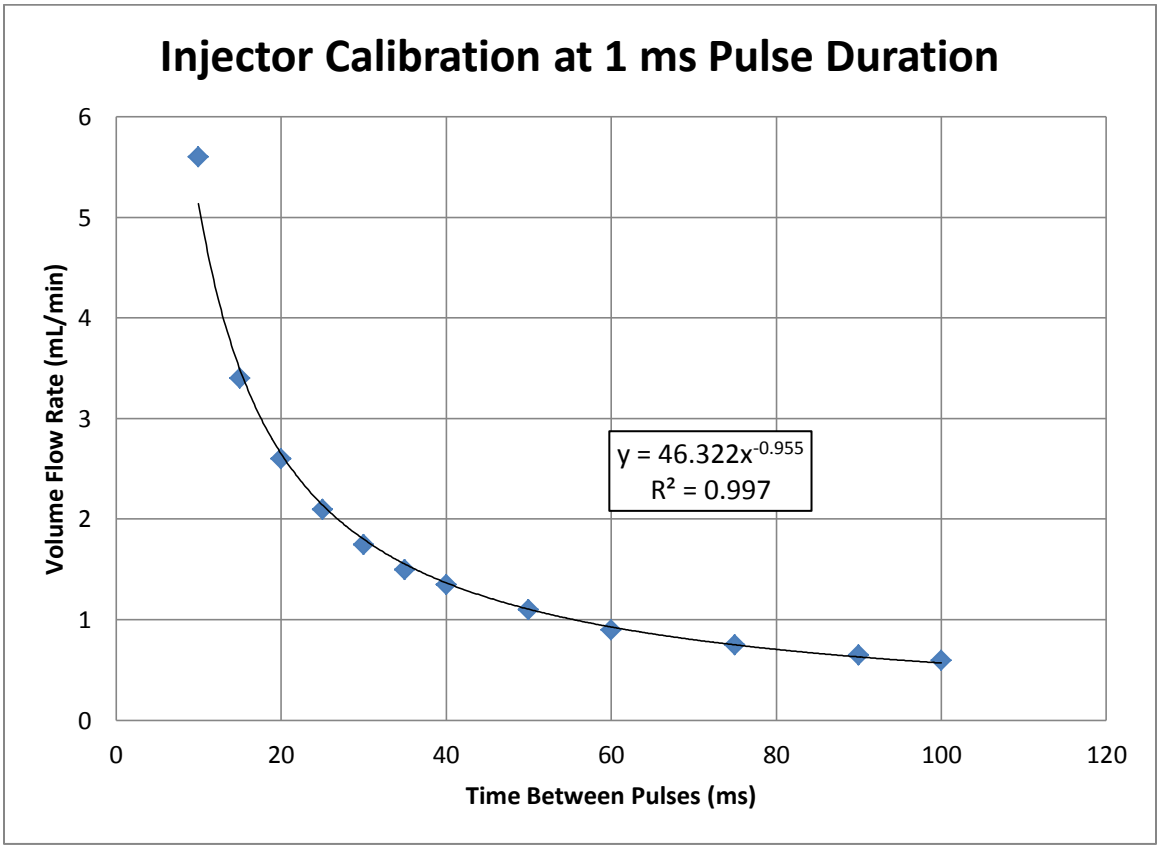

Figure A.1: Plot of flow rate v. time between pulses at a 1 ms pulse duration for the fuel injector operating on kerosene.

A.2 MICROPUMP CALIBRATION

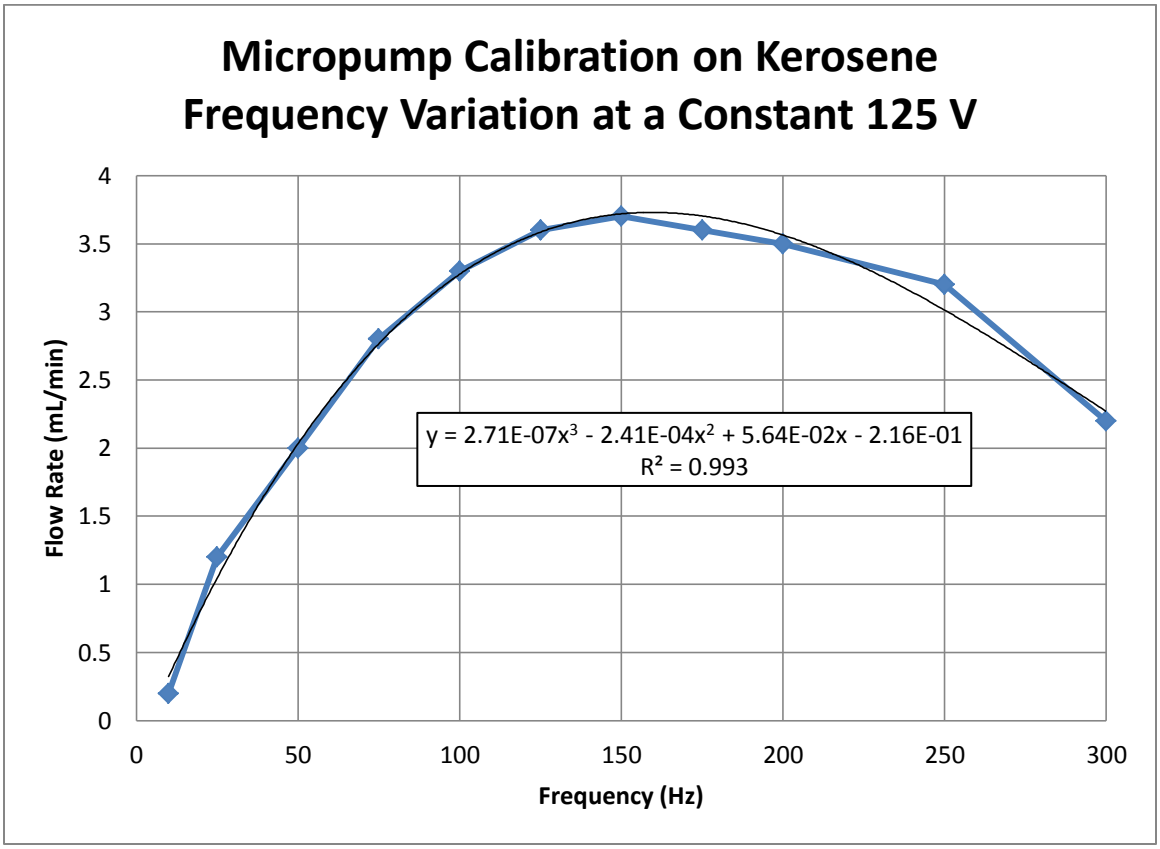

Figure A.2: Plot of flow rate v. input frequency at a constant 125 V for the micropump operating on kerosene.

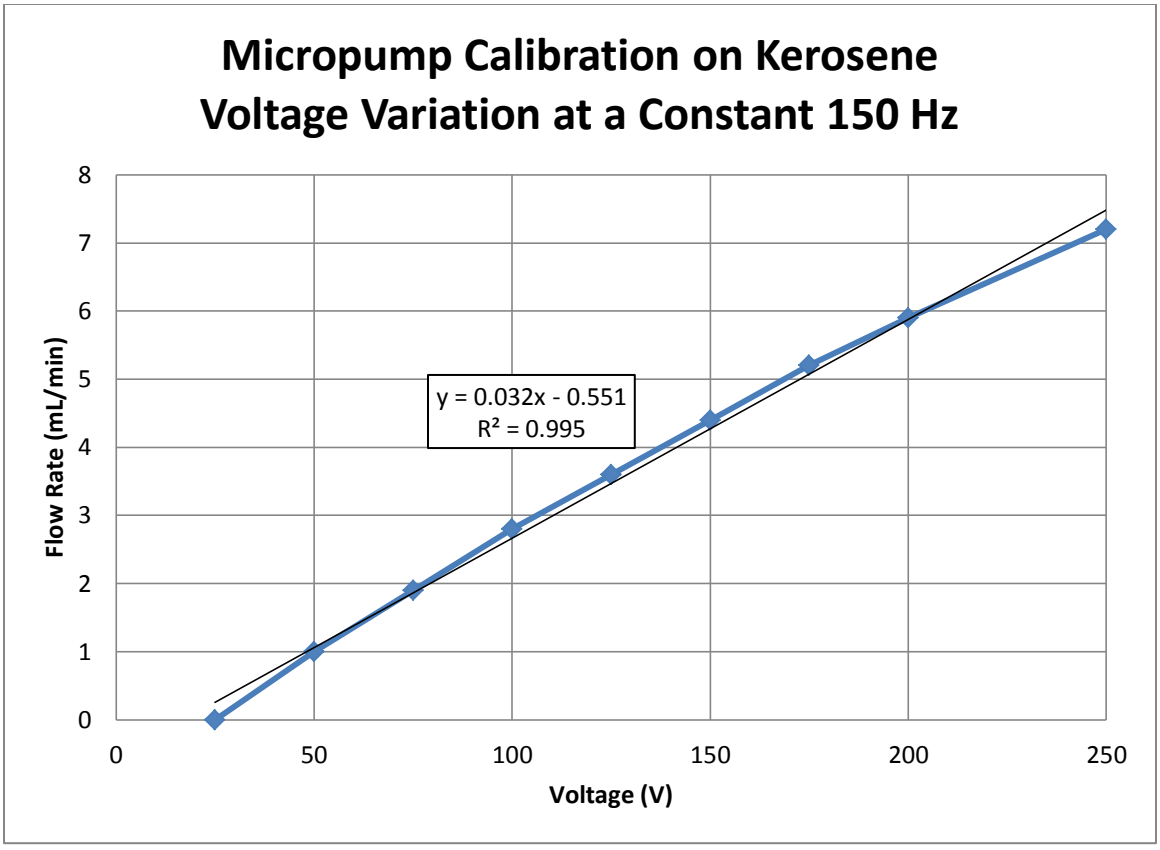

Figure A.3: Plot of flow rate v. input voltage at a frequency of 150 Hz for the micropump operating on kerosene.

A.3 UEGO CALIBRATION

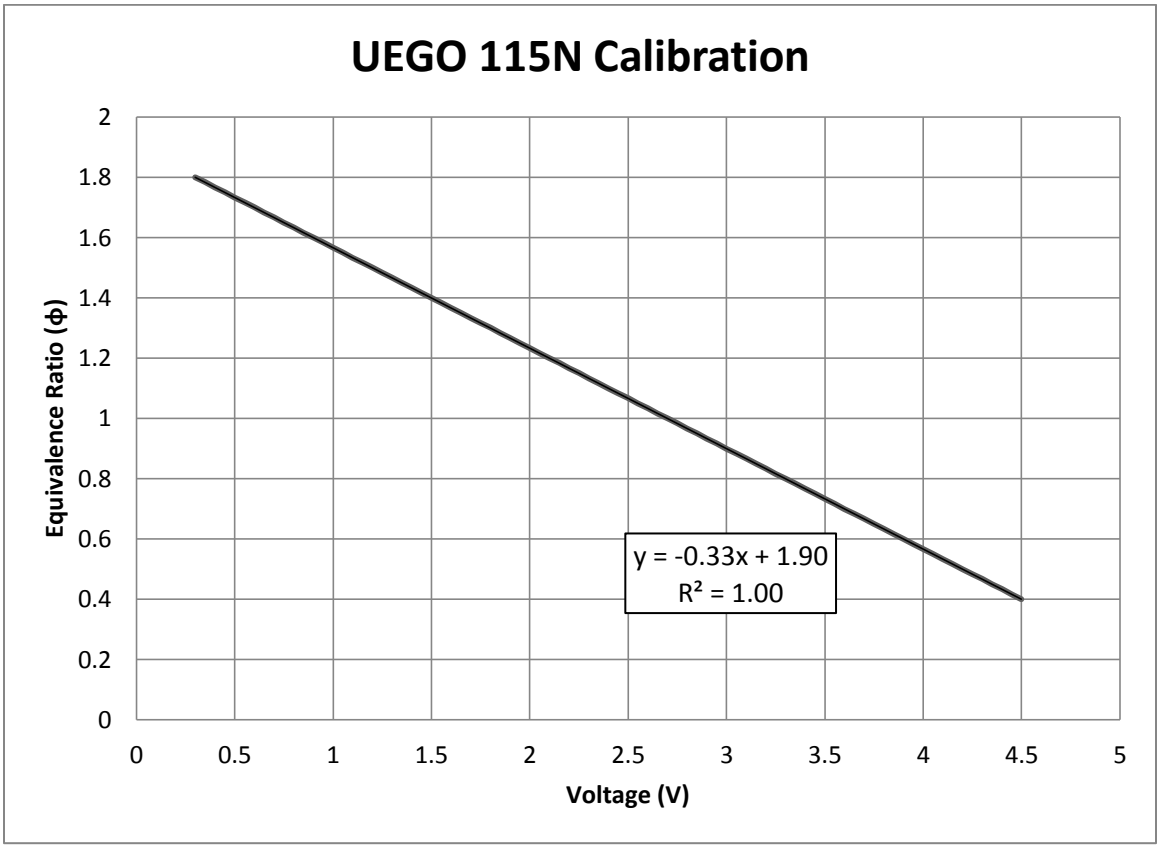

Figure A.4: Plot of equivalence ratio v. output voltage for the UEGO sensor calibrated to the 115N specification.

Appendix B: Heat Exchanger Energy Balance Calculations

The UEGO sensor measured an equivalence ratio of 1.05 for steady state operation of the MSR burner.

$$\phi = 1.05$$

While kerosene is composed of many types of molecules having different lengths and arrangements, it is generally considered that the structural formula can be approximated as alkanes having lengths between C12 and C15 [24]. For this analysis, an alkane of length C14 was assumed. The chemical formula is $C_{14}H_{30}$. In addition, complete combustion was assumed.

The stoichiometric chemical equation was first determined to be:

$$C_{14}H_{30} + 21.5(O_2 + 3.76N_2) \rightarrow 14CO_2 + 15H_2O + 80.84N_2$$

Incorporating the measured equivalence ratio yielded the chemical equation used in this analysis:

$$C_{14}H_{30} + 20.48(O_2 + 3.76N_2) \rightarrow 13.33CO_2 + 14.29H_2O + 76.99N_2 + 0.05C_{14}H_{30}$$

Since the equivalence ratio was measured to be larger than one, the reaction was slightly fuel rich, resulting in some unburned hydrocarbons in the products. However, the amount of excess fuel is so low that the unburned hydrocarbons can be neglected for these efficiency calculations.

The mass flow rate of the fuel was measured to be 0.055 g/sec, and the molecular weight of the assumed fuel formula is 198 g/mol. Then, the molar flow rate of the fuel could be calculated.

$$\dot{n_F} = \frac{\dot{m}_F}{M_F} = \frac{0.055\,\frac{g}{sec}}{198\,\frac{g}{mol}} = 2.78 * 10^{-4}\,\frac{mol}{sec}$$

Then, since it was known from the chemical equation how many moles of each product were produced per mole of fuel combusted, the molar flow rates of the products were calculated.

$$\dot{n}_{CO_2} = 0.0037 \frac{mol}{sec}$$
$$\dot{n}_{H_2O} = 0.004 \frac{mol}{sec}$$
$$\dot{n}_{N_2} = 0.021 \frac{mol}{sec}$$

The energy that was released into the heat exchanger from the combustion of the fuel was calculated. The lower heating value was taken from Table 1.1.

$$\dot{Q}_{in} = \dot{m}_F * LHV = 0.055 \frac{g}{sec} * 43.1 \frac{kJ}{g} = 2371W$$

The energy exiting the heat exchanger was calculated from the following formula:

$$\dot{Q}_{out} = \sum_P \dot{n}_i * h_i^s(T)$$

where $h_i^s(T)$ is the sensible enthalpy at a prescribed temperature of product species i. The sensible enthalpies were taken from [25].

A sample calculation for the 16 inch long heat exchanger with a gas exit temperature of 444.3K is now presented:

$$Q_{out} = 0.0037 \frac{mol}{sec} * 5874.5 \frac{J}{mol} + 0.004 \frac{mol}{sec} * 4979.8 \frac{J}{mol} + 0.021 \frac{mol}{sec} * 4268.4 \frac{J}{mol} = 131W$$

The amount of energy captured by the heat exchanger is the difference between the energy released into the heat exchanger and the energy exiting it. For the 16 inch heat exchanger, that is:

$$\dot{Q}_{HX} = \dot{Q}_{in} - \dot{Q}_{out} = 2371W - 131W = 2240W$$

Finally, the efficiency of the heat exchanger is the amount of energy extracted by the heat exchanger divided by the amount of energy released into the heat exchanger by the combustion of the fuel.

$$\eta_{HX} = \frac{\dot{Q}_{HX}}{\dot{Q}_{in}} = \frac{2240W}{2371W} = 0.945 = 94.5\%$$

Similar calculations were performed for the other length heat exchangers.

Appendix C: Uncertainty Analysis

The main source of uncertainty in the heat exchanger temperature measurements was the accuracy of the thermocouples. Positioning of the hand-held thermocouple probe was also a source of uncertainty for the gas temperature measurements, but unfortunately that was not able to be fully quantified. The gas temperature measurements were repeated several times for various configurations, and produced repeatable results. According to Omega, the K-type thermocouples used in this study have a standard limit of error of the greater of 2.2°C or 0.75% [22]. The heat exchanger temperatures were sufficiently low that the first error limit applied except for some measurements of the 5 inch long heat exchanger close to the burner. The measurement error associated with the transient heating of the 16 inch long heat exchanger with and without attached thermoelectric modules is shown in Figure C.1.

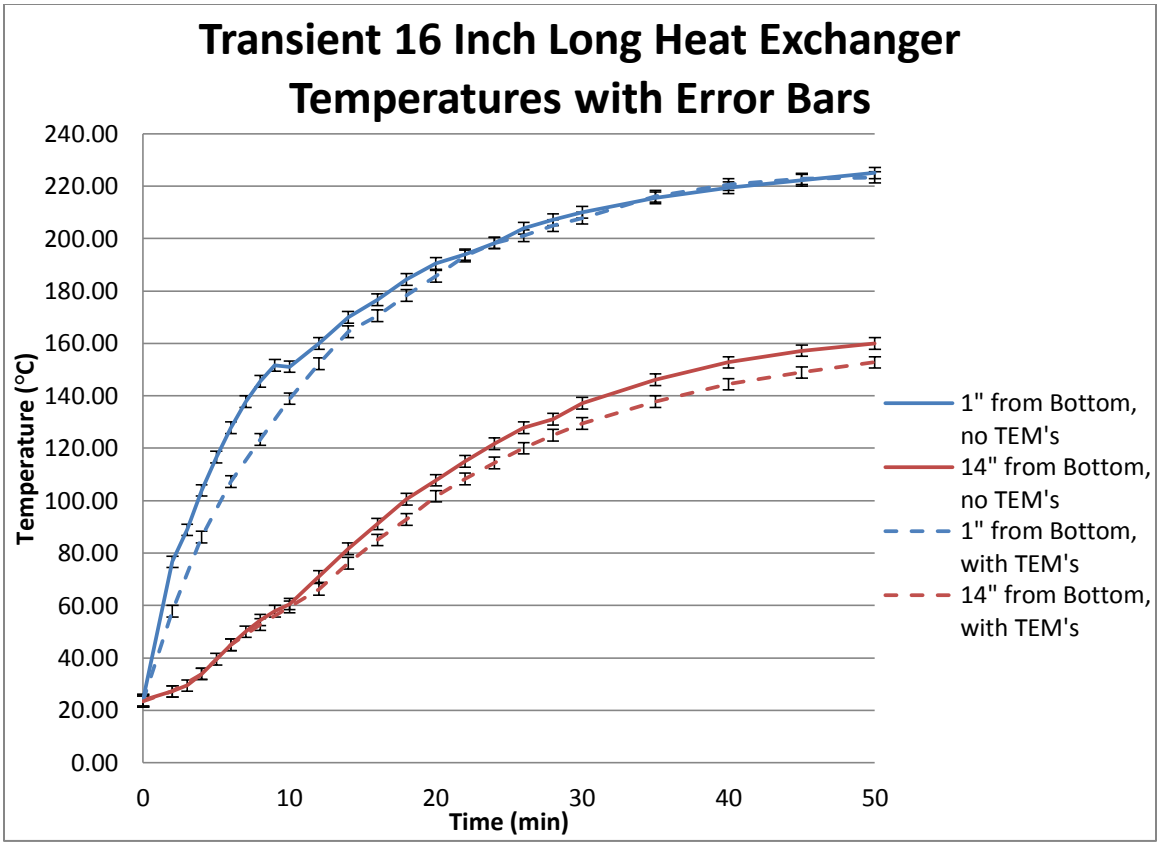

Figure C.1: Plot of transient temperatures of the 16 inch long heat exchanger with and without attached thermoelectric modules taken at the top and bottom thermocouples with error bars.

The error bars overlap for times after about 20 minutes for the 1 inch from bottom measurements, and for times before about 10 minutes for the 14 inches from bottom measurements. The comparison between temperatures during these times may not be statistically significant based on this source of experimental error.

Figure C.2 shows the error associated with the temperature measurements across the width of the 11 inch long heat exchanger for both cases centered over the burner and not centered. Only the accuracy of the thermocouples is incorporated into the error bars.

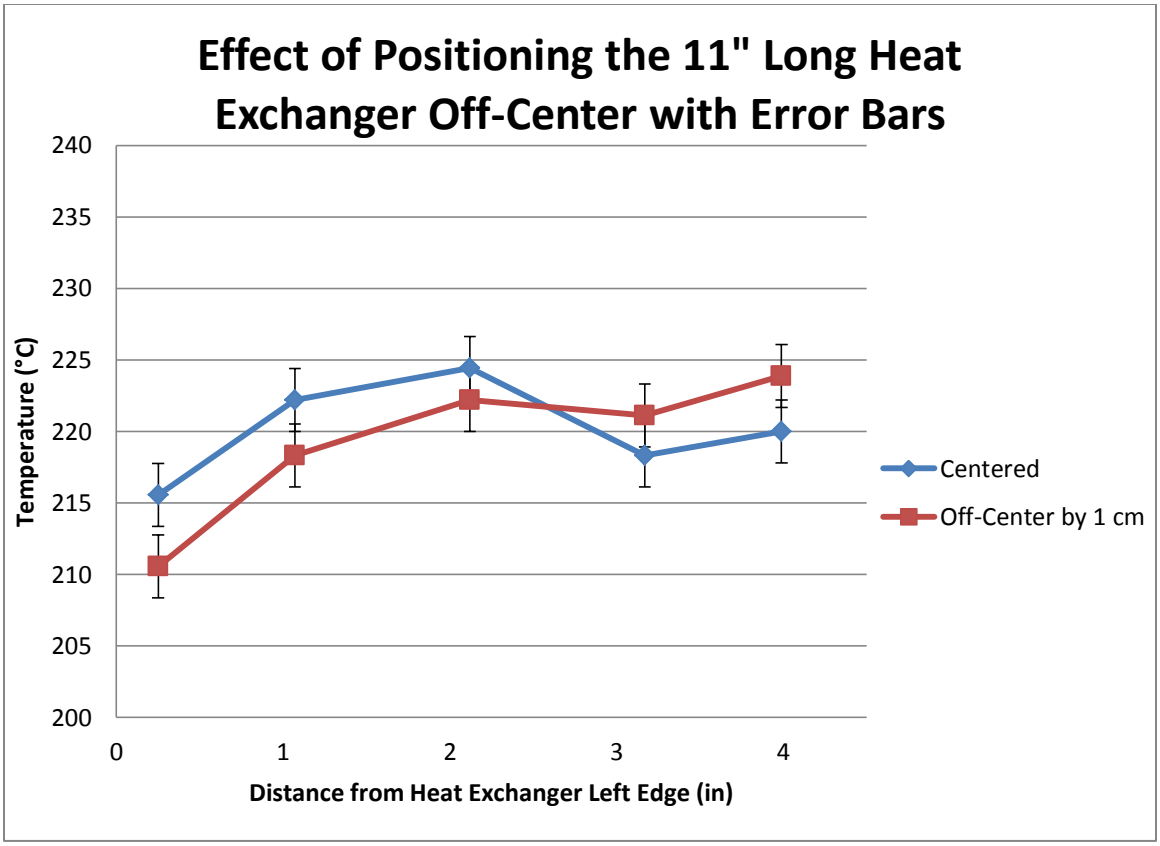

Figure C.2: Plot of the effect on steady-state temperatures across the width of the 11 inch long heat exchanger without attached thermoelectric modules from deliberately positioning it 1 cm to the left with error bars.

The error bars are relatively large compared to the differences in temperatures between the centered and off-center cases. For all points except the leftmost one, the error bars overlap. Therefore, these trends may not be significant.

Appendix D: Measured Temperatures Used to Calculate Averages in Tables 4.2 and 4.3

	Top Edge Temperature (°C)	Bottom Edge Temperature (°C)	Average Temperature (°C)
Passive Cooling, Cold Side	129	139	134
Passive Cooling, Hot Side	209	228	219
Active Cooling, Cold Side	57	55	56
Active Cooling, Hot Side	156	170	163

Table D.1: Chart of measured temperatures at the top and bottom edges of the 5 inch long heat sink and heat exchanger used to calculate the averages in Table 4.2.

	Top Edge Temperature (°C)	Bottom Edge Temperature (°C)	Average Temperature (°C)
Passive Cooling, Cold Side	127	151	139
Passive Cooling, Hot Side	194	226	210
Active Cooling, Cold Side	50	56	53
Active Cooling, Hot Side	153	172	163

Table D.2: Chart of measured temperatures at the top and bottom edges of the 11 inch long heat sink and heat exchanger used to calculate the averages in Table 4.3.

Bibliography

[1] Feynman, R.P. "Plenty of Room at the Bottom," 1959.

[2] Fernandez-Pello, A.C. "Micropower Generation Using Combustion: Issues and Approaches.," *Proceedings of the Combustion Institute*, vol. 29, pp. 883-899, 2002.

[3] Quintiere, J.G., *Fundamentals of Fire Phenomena*. West Sussex, England: John Wiley & Sons Ltd., 1st ed., 2006.

[4] Sadasivuni, V., and Ajay K. Agrawal. "A novel meso-scale combustion system for operation with liquid fuels.," *Proceedings of the Combustion Institute*, vol. 32, pp. 3155-3162, 2009.

[5] Kyritsis, D.C., Ismael Guerrero-Arias, Subir Roychoudhury, and Alessandro Gomez. "Mesoscale Power Generation by a Catalytic Combustor using Electrosprayed Liquid Hydrocarbons.," *Proceedings of the Combustion Institute*, vol. 29, pp. 965-972, 2002.

[6] Huth, J., S.Y. Kim, Ezekiel Holliday, and Andrew Buffalino. "Development of a Wearable JP8-Fueled Soldier Power Source."

[7] Gomez, A., J. Berry, S. Roychoudhury, and J. Huth. "Palm Power: Using Combustion at Small Scales and a Free Piston Stirling Engine to Replace Batteries," 2005.

[8] Kyritsis, D.C., et al. "Optimization of a catalytic combustor using Electrosprayed liquid hydrocarbons for mesoscale power generation.," *Combustion and Flame*, vol. 139, pp. 77-89, 2004.

[9] The United States Department of Labor, Occupational Safety & Health Administration. "Safety and Health Topics: Jet Fuel (JP8)," http://www.osha.gov/dts/chemicalsampling/data/CH_248748.html, 2003.

[10] Military Specification MIL-DTL-83133E. "Turbine Fuels, Aviation, Kerosene Types, NATO F-34 (JP-8), NATO F-35, and JP-8+100," 1999.

[11] Cameo Chemicals. "Kerosene," http://cameochemicals.noaa.gov/chemical/960, 1999.

[12] Bartels Mikrotechnik. "Technical Data mp6," http://www.micro-components.com/index.php/product-information/technical-data.html, 2010.

[13] Watlow Electric Manufacturing Company. "ULTRAMIC Advanced Ceramic Heaters," http://watlow.com/products/heaters/heater1.cfm?pageid=52&famid=10, 2011.

[14] Brunton Inc. "Vapor AF All Fuel Expedition Stove," http://www.brunton.com/product.php?id=428, 2010.

[15] Cascade Designs Inc. "MSR Whisperlite Internationale Multi-Fuel Stove," http://cascadedesigns.com/msr/stoves/expedition-stoves/whisperlite-internationale/product, 2010.

[16] HeatsinkUSA. "4.230 Inch Profile – Parts F001 to F048," http://www.heatsinkusa.com/storename/heatsinkusa/Image-10607166.aspx?, 2011.

[17] Bijjula, K., E.D. Wetzel, and D.G. Vlachos. "Optimizing Efficiency of Coupled Thermoelectric/Thermal Source Devices."

[18] Federici, J.A., et al. "Catalytic microcombustors with integrated thermoelectric elements for portable power production.," *Journal of Power Sources*, vol. 161, pp. 1469-1478, 2006.

[19] Marlow Industries, Inc. "Power Generators," http://www.marlow.com/power-generators/, 2008.

[20] Bartels Mikrotechnik. "Questions and Answers," http://www.micro-components.com/index.php/support/qaa.html, 2010.

[21] Cotronics Corp. "3000°F Ceramic Papers," http://www.cotronics.com/vo/cotr/fc_papers.htm, 2008.

[22] Omega Engineering, Inc. "Selection Guide: Thermocouple," http://www.omega.com/guides/thermocouples.html, 2010.

[23] Incropera, F.P., and David P. DeWitt, *Fundamentals of Heat and Mass Transfer.* New Jersey: John Wiley & Sons, Inc., 5th ed., 2002.

[24] Ebbing, D.D., and Steven D. Gammon, *General Chemistry*. Massachusetts: Houghton Mifflin Company, 9th ed., 2009.

[25] Ohio University. "Combustion Molar Enthalpy Tables," http://www.ohio.edu/mechanical/thermo/property_tables/combustion/index.html, 2009.

Vita

Ross Michael Rechen was born in Manhasset, New York. He grew up in Plainview, New York and attended Plainview-Old Bethpage John F. Kennedy High School. Afterward, he attended Penn State University and received a Bachelor of Science degree in Mechanical Engineering. Following graduation, Ross found employment at Exergy LLC in Garden City, New York, which is a small company that manufactures miniature heat exchangers. He then attended the University of Texas at Austin to work towards a Master's degree in Mechanical Engineering. His graduate focus was Thermal / Fluid Systems, and he earned his degree in May 2011. He hopes to find employment in the aerospace industry or any other where he may contribute using his knowledge and expertise in heat transfer.

Email: rrechen@gmail.com

This thesis was typed by Ross Michael Rechen.